M 2020

U.PORTO
FEUP FACULDADE DE ENGENHARIA
UNIVERSIDADE DO PORTO

DEVELOPMENT OF NANOSTRUCTURED CARBON SPHERES FOR ENVIRONMENTAL APPLICATIONS

ANA LUÍSA SANTOS VIEIRA

MASTER DISSERTATION PRESENTED
TO THE FACULTY OF ENGINEERING OF THE UNIVERSITY OF PORTO IN
CHEMICAL ENGINEERING

Master in Chemical Engineering

Development of nanostructured carbon spheres for environmental applications

Master dissertation

of

Ana Luísa Santos Vieira

Developed within the course of dissertation

held in

Associate Laboratory LSRE-LCM — Laboratory of Separation and Reaction Engineering — Laboratory of Catalysis and Materials

Supervisor at FEUP: **Dr. Ana Rita Lado Teixeira Ribeiro**
Co-supervisors at FEUP: **Prof. Adrián Manuel Tavares da Silva**
Dr. Rui Sérgio da Silva Ribeiro

U.PORTO
FEUP FACULDADE DE ENGENHARIA UNIVERSIDADE DO PORTO
DEPARTAMENTO DE ENGENHARIA QUÍMICA

July 2021

CLASSIFIED DOCUMENT. USE ONLY FOR EVALUATION PURPOSES.

Acknowledgments

The realization of this dissertation integrated in the Master in Chemical Engineering was only possible due to the friendship, collaboration and willingness of many people, from colleagues and teachers, to my family and friends, who directly or indirectly supported me along the entire journey. Hence, I would like to express my sincere gratitude:

To my supervisors, Dr. Rita Ribeiro, Dr. Rui Ribeiro and Prof. Adrián Silva, my sincere thanks for the opportunity, availability, and attention throughout this period, and for all the knowledge transmitted that made possible the development and contribution to my academic training.

To all LSRE-LCM team, a special thanks for their hospitality, for the good environment created and for the help provided throughout this time. I also want to thank my colleagues Inês, Lino and Mariana for all the help, good times, and shared conversations.

I am especially thankful to my parents for all the affection, support, encouragement, and emotional and financial support throughout the entire journey. I also want to thank my sister Joana for allowing me moments of happiness and fun in the most difficult and stressful times of this task.

To all my friends, who helped me directly or indirectly in this moment of my academic trajectory, for their companionship, loyalty and sharing of experiences.

This work was financially supported by: Project PTDC/QUI-QAN/30521/2017 - POCI-01-0145-FEDER-030521 - funded by FEDER funds through COMPETE2020 - Programa Operacional Competitividade e Internacionalização (POCI) and by national funds (PIDDAC) through FCT/MCTES. We would also like to thank the scientific collaboration under Base Funding - UIDP/50020/2020 of the Associate Laboratory LSRE-LCM - funded by national funds through FCT/MCTES (PIDDAC). ARLR acknowledges FCT funding under DL57/2016 Transitory Norm Programme. Technical assistance with SEM analysis is gratefully acknowledged to CEMUP team.



Abstract

The removal of organic micropollutants (OMPs) from water matrices have been attracting increasing attention, with a special focus on adsorbents with increasingly superior performance.

This study aims to explore the potential to synthesize, characterize and apply hollow carbon spheres (CSs) as adsorbent materials. To achieve this goal, silica@polymer spheres with a core@shell structure were synthesized, and then thermally treated at 800 ºC to obtain silica@carbon spheres (SiO_2@CSs). By removing the core through dissolution of silica, hollow carbon spheres were obtained. Accordingly, three types of samples of both SiO_2@CSs and CSs were prepared by varying the ethanol/water volumetric ratio (2, 4.5 and 7) employed in the first stage of their synthesis (*i.e.*, during the application of the Stöber's method to obtain silica particles). Scanning electron microscopy coupled to energy-dispersive X-ray spectroscopy (SEM-EDS) was then used to study the morphology and particle size distribution of the synthesized materials, and the effectiveness of the silica core removal. Thermogravimetric analysis (TGA) was used to estimate the carbon content. The textural properties were determined from nitrogen adsorption-desorption isotherms obtained at -196 ºC, whereas the surface chemistry characterization comprised the determination of the pH at the point of zero charge (pH_{PZC}). Adsorption kinetic and equilibrium studies were then carried out employing diclofenac and venlafaxine as model OMPs. Kinetic (fractional power, pseudo-first order, pseudo-second order and Elovich) and equilibrium (Langmuir, Freundlich and Sips) models were fit to the experimental data.

All the synthesized materials exhibited a spherical morphology, the particle size increasing with the ethanol/water volumetric ratio. Silica removal was not effective for all the CSs (TGA residue ranging from 3 to 46 wt.%). The average diameter of the SiO_2@CSs varied from 168 to 270 nm and the dominant element was silicon, while the CSs had an average diameter of 109 to 284 nm and carbon as the dominant element. The specific surface area (S_{BET}) of the CSs ranged from 271 to 602 $m^2\ g^{-1}$, making them more porous compared to SiO_2@CSs (S_{BET} in the range 115 to 144 $m^2\ g^{-1}$). The pH_{PZC} of the CSs ranged from 8 to 10, revealing their basic character. From the kinetic studies, it was possible to demonstrate the positive effect of having a hollow core, *i.e.*, of removing the silica core. Equilibrium studies demonstrated that CSs prepared with an ethanol/water volumetric ratio of 7 were the best performing CSs when considering both OMPs. Moreover, adsorption kinetic data was well described by the pseudo-first order and power fractional kinetic models for diclofenac and for venlafaxine, respectively, whereas the Sips model fitted well to the equilibrium data.

Keywords: Silica-carbon spheres, Hollow spheres, Diclofenac, Venlafaxine, Adsorption.

Resumo

A remoção de micropoluentes orgânicos (OMPs) de matrizes aquosas tem vindo a atrair uma atenção crescente, com um foco especial em adsorventes com desempenho superior.

Este estudo visa explorar o potencial da síntese, caracterização e aplicação de esferas ocas de carbono (CSs) como adsorventes. Nesse sentido, sintetizaram-se esferas de sílica@polímero com uma estrutura de núcleo@carapaça, que depois foram sujeitas a tratamento térmico a 800 ºC para se obter esferas de sílica@carbono (SiO_2@CSs). Ao remover o núcleo através da dissolução da sílica obteve-se as CSs. Assim, foram preparadas três tipos de amostras de SiO_2@CSs e CSs, variando a razão volumétrica de etanol/água (2, 4,5 e 7), que foi utilizada na primeira fase da síntese (ou seja, durante a aplicação do método de Stöber para se obter partículas de sílica). A microscopia eletrónica de varrimento acoplada à espetroscopia por dispersão de energia de raios-X (SEM-EDS) foi utilizada para estudar a morfologia e distribuição de tamanhos das partículas sintetizadas, e a eficácia da remoção do núcleo de sílica. A análise termogravimétrica (TGA) foi utilizada para estimar o teor de carbono. As propriedades texturais foram obtidas a partir de isotérmicas de adsorção-dessorção de azoto a -196 ºC, enquanto a caracterização química de superfície incluiu a determinação do pH no ponto de carga zero (pH_{PZC}). Realizou-se estudos cinéticos e de equilíbrio de adsorção utilizando diclofenac e venlafaxina como compostos modelos de OMPs. Os modelos cinéticos (poder fracionário, pseudo-primeira ordem, pseudo-segunda ordem e Elovich) e de equilíbrio (Langmuir, Freundlich e Sips) foram ajustados aos dados experimentais.

Todos os materiais sintetizados exibiram uma morfologia esférica e os seus tamanhos aumentaram com a razão volumétrica de etanol/água. A remoção de sílica não foi eficaz para todas as CSs (resíduos de TGA de 3 a 46% m/m). O diâmetro médio das SiO_2@CSs variou de 168 a 270 nm e o elemento dominante foi o silício, já o diâmetro médio das CSs variou de 109 a 284 nm e o carbono foi o elemento dominante. A área de superfície específica (S_{BET}) das CSs variou entre 271 a 602 $m^2\ g^{-1}$, revelando que são mais porosas em comparação com as SiO_2@CSs (S_{BET} de 115 a 144 $m^2\ g^{-1}$). O pH_{PZC} das CSs variou de 8 e 10, mostrando o seu caracter básico. A partir dos estudos cinéticos demonstrou-se o efeito positivo de se ter um núcleo oco, ou seja, de se remover o núcleo de sílica. Os estudos de equilíbrio indicaram que as CSs preparadas com uma razão volumétrica de etanol/água de 7 tiveram melhor desempenho quando se consideram ambos os OMPs. Além disso, os dados da cinética de adsorção foram bem descritos pelos modelos de pseudo-primeira ordem e poder fracionário, para o diclofenac e para a venlafaxina, respetivamente, enquanto o modelo Sips se ajustou bem aos dados de equilíbrio.

Palavras-chave: Esferas de sílica-carbono, Esferas ocas, Diclofenac, Venlafaxina, Adsorção.

Declaration

I hereby declare, under word of honor, that this work is original and that all non-original contributions are indicated, and due reference is given to the author and source.

Porto, July 5th, 2021

Ana Luísa Santos Vieira

Index

Acknowledgments i
Abstract ii
Resumo iii
Declaration iv
Index v
List of figures vii
List of tables viii
Notation and Glossary ix
1. Introduction 1
1.1. Framing and presentation of the work 1
1.2. Presentation of research group 1
1.3. Contribution of the author to the work 1
1.4. Organization of the dissertation 2
2. Context and state-of-the-art 3
2.1. Micropollutants in the environment 3
2.1.1. European Union water legislation and reference documents 4
2.1.2. Origin, distribution, and fate 5
2.1.3. Ecosystem and human health risks 5
2.2. Occurrence of pharmaceuticals in the environment 6
2.2.1. Diclofenac 8
2.2.2. Venlafaxine 8
2.3. Nanostructured carbon materials for adsorption 8
3. Materials and methods 11
3.1. Chemicals and instruments 11
3.2. Synthesis of CSs 11
3.3. Characterization techniques 12
3.4. Kinetic and equilibrium adsorption experiments 13
3.4.1. Modeling studies 13

3.5. Analytical procedures 16
4. Results and discussion 17
4.1. Mechanistic insights into the synthesis of CSs 17
4.2. Characterization of CSs 20
4.2.1. Scanning electron microscopy 20
4.2.2. Thermogravimetric analysis 24
4.2.3. Textural characterization 26
4.2.4. Surface chemistry characterization 27
4.3. Kinetic adsorption experiments 28
4.4. Equilibrium adsorption experiments 32
5. Conclusions 37
6. Assessment of the work 39
6.1. Objectives achieved 39
6.2. Other work carried out 39
6.3. Final assessment 40
References 41
Appendix A — Synthesis of CSs 45
Appendix B — Characterization techniques 46
Appendix C — Calibration curves 50
Appendix D — Kinetics adsorption data 53
Appendix E — Equilibrium adsorption data 55

List of figures

Figure 2.1. WFD implementation milestones and policy developments since its adoption (2000–2027) (EAP: Community Environmental Action Programmes). 4
Figure 4.1. Schematic representation of the synthesis of hollow CSs. 18
Figure 4.2. Pictures taken during the synthesis of SiO_2@RF spheres. 19
Figure 4.3. Pictures of (a) SiO_2@RF and (b) SiO_2@CSs. 20
Figure 4.4. SEM micrographs of: (a) $SiO_2@CS_2$, (b) CS_2, (c) $SiO_2@CS_{4.5}$, (d) $CS_{4.5}$, (e) $SiO_2@CS_7$, and (f) CS_7. Images obtained in SE mode. 21
Figure 4.5. Particle diameter of SiO_2@CSs and CSs as a function of the E/W ratio. 22
Figure 4.6. SEM micrographs of: (a) $SiO_2@CS_2$, (b) CS_2, (c) $SiO_2@CS_{4.5}$, (d) $CS_{4.5}$, (e) $SiO_2@CS_7$, and (f) CS_7. Images obtained in BSE mode. 23
Figure 4.7. EDS spectra of: (a) $SiO_2@CS_2$ and CS_2, (b) $SiO_2@CS_{4.5}$ and $CS_{4.5}$ and (c) $SiO_2@CS_7$ and CS_7. Data obtained over a global area of each sample. 24
Figure 4.8. TGA and DTGA curves in oxidative (air) atmosphere: (a) $SiO_2@CS_2$, (b) CS_2, (c) $SiO_2@CS_{4.5}$, (d) $CS_{4.5}$, (e) $SiO_2@CS_7$ and (f) CS_7. 25
Figure 4.9. Kinetic experimental and theoretical data for the adsorption of DCF and VFX onto CS_2. Experiments performed with $[CS_2]$ = 0.25 g L^{-1}, $[DCF]_0$ or $[VFX]_0$ = 100 mg L^{-1}, pH = 6.4 or 6.2 (inherent pH of DCF and VFX solutions, respectively), T = 23 ± 1 ºC (room temperature), and stirring speed of 200 rpm. 29
Figure 4.10. Kinetic experimental and theoretical data for the adsorption of DCF and VFX onto $SiO_2@CS_2$. Experiments performed with $[SiO_2@CS_2]$ = 1.28 g L^{-1} (corresponding to $C_{ads,C}$ = 0.2425 g L^{-1}), $[DCF]_0$ or $[VFX]_0$ = 100 mg L^{-1}, pH = 6.4 or 6.2 (inherent pH of DCF and VFX solutions, respectively), T = 23 ± 1 ºC (room temperature), and stirring speed of 200 rpm. 31
Figure 4.11. Experimental and theoretical data for the adsorption isotherms of (a) DCF and (b) VFX onto CS_2, $CS_{4.5}$ or CS_7. Experiments performed with $[CS_X]$ = 0.25 g L^{-1}, $[DCF]_0$ or $[VFX]_0$ = 1, 5, 10, 25, 50, 75, and 100 mg L^{-1}, T = 23 ± 1 ºC (room temperature), t = 24 h, and stirring speed of 200 rpm. 32
Figure B.1. Histogram of particle size distribution of: (a) $SiO_2@CS_2$, (b) CS_2, (c) $SiO_2@CS_{4.5}$, (d) $CS_{4.5}$, (e) $SiO_2@CS_7$, and (f) CS_7 as determined by SEM measurements. Red curves represent a log-normal distribution. 47
Figure B.2. Nitrogen adsorption-desorption isotherms at – 196 ºC of: (a) $SiO_2@CS_2$, (b) CS_2, (c) $SiO_2@CS_{4.5}$, (d) $CS_{4.5}$, (e) $SiO_2@CS_7$, and (f) CS_7. 48
Figure B.3. Plot of final pH versus initial pH for determination of the pH_{PZC} of: (a) CS_2, (b) $CS_{4.5}$, and (c) CS_7. 49
Figure C.1. Chromatogram for a two-component mixture of the detector signal (μV) as a function of time (min). 50

List of tables

Table 2.1. Physicochemical and pharmacological properties of DCF and VFX. 7
Table 4.1. Average diameters ($d_{average}$) of the tested materials and their associated standard deviations. 22
Table 4.2. TGA residues and carbon content of the CSs, as determined by TGA under air atmosphere. 26
Table 4.3. Specific surface area (S_{BET}), non-microporous surface area (S_{Meso}), micropore volume (V_{Micro}) and total pore volume (V_{Total}) of the CSs. 27
Table 4.4. pH at the point of zero charge (pH_{PZC}) data of the CSs. 27
Table 4.5. Kinetic model parameters (non-linearized form equations) for the adsorption of DCF and VFX onto CS_2. 29
Table 4.6. Solution pH, p*K*a of each OMP, and pH_{PZC} of CS_2. 30
Table 4.7. Kinetic model parameters (non-linearized form equations) for the adsorption of DCF and VFX onto SiO_2@CS_2. 31
Table 4.8. Equilibrium model parameters (non-linearized form equations) for the adsorption of DCF and VFX onto the hollow CSs. 33
Table 4.9. Comparison of the performance of several reported carbon-based materials developed as adsorbents of DCF. 35
Table 4.10. Comparison of the performance of several reported carbon-based materials developed as adsorbents of VFX. 36
Table A.1. Amounts of reactants used in the synthesis of the SiO_2@RF spheres. 45
Table C.1. Correlation coefficient (r^2), limit of detection (LOD) and limit of quantitation (LOQ). 51
Table C.2. Repeatability of the method. 52
Table C.3. Intermediate precision for the analysis of VFX in standard solutions (3 days, 3 replicates per day). 52
Table C.4. Intermediate precision for the analysis of DCF in standard solutions (3 days, 3 replicates per day). 52
Table D.1. Average concentration (C), average adsorption capacity (q_t) and its standard deviation (σ), and removal efficiency (E) for CS_2 in DCF and VFX solutions. Experiments performed with C_{ads} = 0.25 g L^{-1}, pH = 6.4 or 6.2 (inherent pH of DCF and VFX solutions, respectively), T = 23 ± 1 ºC (room temperature), and stirring speed of 200 rpm. 53
Table D.2. Average concentration (C), average adsorption capacity (q_t) and its standard deviation (σ), and removal efficiency (E) for SiO_2@CS_2 in DCF and VFX solutions. Experiments performed with C_{ads} = 1.28 g L^{-1} (corresponding to $C_{ads,C}$ = 0.2425 g L^{-1}), pH = 6.4 or 6.2 (inherent pH of DCF and VFX solutions, respectively), T = 23 ± 1 ºC (room temperature), and stirring speed of 200 rpm. 54
Table E.1. Initial concentration (C_0), equilibrium concentration (C_e), equilibrium adsorption (q_e), and removal efficiency (E) for CS_2, $CS_{4.5}$ and CS_7 in DCF and VFX solutions. Experiments performed with C_{ads} = 0.25 g L^{-1}, T = 23 ± 1 ºC (room temperature), t = 24 h, and stirring speed of 200 rpm. 55

Notation and Glossary

a	Adjustment parameter of fractional power function model	mg g^{-1} h^{-1}
A	Area	a.u.
$A_{average}$	Average area	a.u.
b	Adjustment parameter of fractional power function model	mg g^{-1} h^{-1}
BO	Burn-off	%
C_0	Initial concentration	mg L^{-1}
C	Concentration	mg L^{-1}
C_{ads}	Adsorbent concentration	g L^{-1}
$C_{ads,C}$	Adsorbent concentration based on the carbon content	g L^{-1}
CC	Carbon content estimated from TGA	
C_e	Equilibrium concentration of adsorbate in the solution	mg L^{-1}
C_t	Adsorbate concentration at a given time "t"	mg L^{-1}
$d_{average}$	Average diameter	nm
E	Removal efficiency	%
k_1	Pseudo-first order model rate constant	h^{-1}
k_2	Pseudo-second order adsorption rate constant	g mg^{-1} h^{-1}
K_F	Freundlich constant	L^{1/n_F} mg^{1-1/n_F} g^{-1}
K_L	Langmuir adsorption constant	L mg^{-1}
K_s	Sips isotherm model constant	L^{n_S} mg^{-n_S}
LOD	Limit of detection	µg L^{-1}
Log K_{ow}	Logarithm of octanol-water partition coefficient	
LOQ	Limit of quantitation	µg L^{-1}
m_{ads}	Mass of adsorbent	g
m_{CS}	Mass of CS	g
$m_{SiO_2@CS}$	Mass of SiO_2@CS	g
$m_{SiO_2@RF}$	Mass of SiO_2@RF	g
MW	Molecular weight	g mol^{-1}
n_F	Adsorption intensity or degree of heterogeneity of the surface	
n_S	Heterogeneity of the adsorption system	
pKa	Acid dissociation constant	
pH	Logarithm of the reciprocal of the hydrogen ion activity	
pH_{PZC}	pH at the point of zero charge	
q_e	Equilibrium adsorption capacity	mg g^{-1}
q_m	Maximum adsorption capacity	mg g^{-1}
q_{sat}	Maximum adsorption capacity in the monolayer	mg g^{-1}
q_t	Adsorption capacity at a given time "t"	mg g^{-1}
r^2	Correlation coefficient	
RSD	Relative standard deviation	%
S_{BET}	Specific surface area	m^2 g^{-1}
S_{Meso}	Non-microporous specific surface area	m^2 g^{-1}
T	Temperature	ºC
t	Time	h
V	Solution volume	mL
V_{NaOH}	Volume of NaOH solution	mL
V_{ads}	Adsorbed volume	cm^3 g^{-1}
V_{Total}	Total specific pore volume	cm^3 g^{-1}
V_{Micro}	Volume of micropores	cm^3 g^{-1}

Greek Letters

α	Initial adsorption rate	g mg^{-1} h^{-1}
β	Desorption constant	mg g^{-1} h^{-1}
$\lambda_{em.}$	Emission wavelength	nm
$\lambda_{exc.}$	Excitation wavelength	nm
$\lambda_{max.}$	Maximum wavelength	nm
σ	Standard deviation	mg g^{-1}

Indexes

X	Ethanol/water volume ratio considered during the synthesis procedure

List of Acronyms

BET	Brunauer–Emmett–Teller
BSE	Backscattered electron
CECs	Contaminants of emerging concern
CSs	Carbon spheres
DTGA	First derivate of the thermogravimetric analysis curve
DCF	Diclofenac
DWTPs	Drinking water treatment plants
EAP	Community Environmental Action Programmes
EDS	Energy-dispersive X-ray spectroscopy
EQS	Environmental quality standards
EU	European Union
E/W	Ethanol/water
F	Formaldehyde
HPLC	High-performance liquid chromatography
HS	Hydroxymethyl-substituted
NMs	Nanomaterials
NSAIDs	Non-steroidal anti-inflammatory drugs
OMPs	Organic micropollutants
PTFE	Polytetrafluoroethylene
PSs	Priority substances/classes
R	Resorcinol
RF	Resorcinol-formaldehyde
SEM	Scanning electron microscopy
SEM-EDS	Scanning electron microscopy coupled to energy-dispersive X-ray spectroscopy
SE	Secondary electron
SNRIs	Serotonin–norepinephrine reuptake inhibitors
TEOS	Tetraethyl orthosilicate
TGA	Thermogravimetric analysis
VFX	Venlafaxine
WFD	Water Framework Directive
WWTPs	Wastewater treatment plants

1. Introduction

1.1. Framing and presentation of the work

Life on Earth fully depends on water, hence the constant search to improve water quality is a vital matter. Organic micropollutants (OMPs), such as pharmaceuticals, contribute to water pollution even when occurring at trace amounts in aquatic compartments. Therefore, there is a need for the elimination of these compounds from the aquatic environment. Bearing this in mind, the main goal of this work is to explore the potential to develop hollow carbon spheres (CSs) as highly efficient adsorbent materials. Accordingly, the following specific objectives were set:

1. Synthesis of nanostructured carbon spheres (CSs) with hollow core and with different particle sizes;
2. Characterization of the CSs;
3. Evaluation of the performance of the CSs in the adsorption of the two selected OMPs;
4. Study the effect of the hollow core, within the CSs, on the adsorption performance;
5. Determination of the time needed to reach the adsorption equilibrium;
6. Study of the effect of particle size on the adsorption performance.

1.2. Presentation of research group

This project was carried out in the "Catalysis and Carbon Materials" Group of Associate Laboratory LSRE-LCM, which is a partnership between LSRE – Laboratory of Separation and Reaction Engineering and LCM – Laboratory of Catalysis and Materials. The main location of LSRE-LCM is in the Department of Chemical Engineering at FEUP - Faculdade de Engenharia da Universidade do Porto.

1.3. Contribution of the author to the work

In this dissertation, I developed nanostructured CSs composed by a hollow core and a carbon shell. I have carried out all the synthesis steps needed to obtain such spherical structures for several times, both to obtain enough of each sample and CSs with different sizes. Specifically, I synthesized CSs with increasing diameter by varying one of the synthesis parameters, namely the ethanol/water volumetric ratio. I also performed the characterization of all the materials, including morphological, textural, and surface chemistry properties. The exception was scanning electron microscopy coupled to energy-dispersive X-ray spectroscopy (SEM-EDS),

which was carried out by the CEMUP team. Nevertheless, I have prepared the samples to be analyzed by SEM-EDS and I carried out all the data interpretation. Moreover, I have performed all the tasks needed to explore the potential of the nanostructured CSs for adsorption processes, including kinetic and equilibrium adsorption studies/modelling. The high-performance liquid chromatography method used for the determination of the two selected OMPs was developed by my supervisor, Dr. Rita Ribeiro. However, I have prepared all the standard solutions, performed the method's calibration, and implemented the methodology on a daily basis for the analysis of the samples collected during the adsorption experiments.

1.4. Organization of the dissertation

This dissertation consists of 6 chapters and 5 appendices. Chapter 1 is the introductory chapter, referring to the framework, presentation of the research group and contributions of the work, and organization of the dissertation.

A general overview of the context and the state-of-the-art is provided in chapter 2, focusing on the application of nanostructured CSs for the adsorption of OMPs.

The materials and methods used for the synthesis, characterization, and application of nanostructured CSs, as well as the analytical method are detailed in chapter 3.

The results are presented and discussed in chapter 4, focusing on the characterization of the CSs, as well as their application in kinetic and equilibrium adsorption studies.

The main conclusions of this study are summarized in chapter 5. The critical analysis of the work done is presented in chapter 6, together with some recommendations for future developments of the work.

2. Context and state-of-the-art

2.1. Micropollutants in the environment

Over the last few decades, the occurrence of pollutants in the aquatic environment has raised increasing interest and concern due to the possible impact on wildlife and human health. Both natural and anthropogenic organic substances, some of those difficult to eliminate by conventional water and wastewater treatment processes [1,2], are constantly released into the environment, thus affecting the chemical status of the Earth's water quality.

Organic micropollutants (OMPs) are usually present in aquatic compartments at trace concentrations, ranging from ng L^{-1} to µg L^{-1} levels or even lower, at pg L^{-1}, reason why they are known as micropollutants [2]. Among these are food additives, industrial and household chemicals, pharmaceuticals and personal care products [2,3]. These OMPs are responsible for altering the endocrine function of many organisms and may originate carcinogenic effects on the aquatic and terrestrial organisms [3].

Conventional wastewater treatment plants (WWTPs) are crucial in urban water systems. They employ a series of treatment stages to clean wastewaters, so that the treated waters achieve the desired quality or required discharge standards, which are defined by national laws. In the case of European Union (EU) member States, the national regulations are set up in compliance with EU law. However, WWTPs usually have limited capacity to remove OMPs. As result, WWTPs are consensually recognized as a common source of OMPs in aquatic systems [3].

The first stage in WWTPs is the preliminary treatment, which aims only at the removal of coarse solids. The subsequent stage is the primary treatment, which aims to remove settleable solids and the floating fraction of the organic matter. In these two stages, physical mechanisms are predominant. In the secondary treatment, the main objective is to remove the organic matter, nitrogen, and phosphorus. This is typically accomplished by biological processes followed by sedimentation, but chemical mechanisms may also be employed. Finally, a tertiary treatment, also called water polishing, may be used as an additional step to further improve the quality of the effluent [4]. The physical mechanisms include screening, mixing, flocculation, sedimentation, flotation, or filtration; the chemical mechanisms comprise precipitation, adsorption, disinfection; and the biological mechanisms can be employed to remove of organic matter, and achieve nitrification/denitrification [4]. Some of these mechanisms can occur simultaneously in the same treatment unit.

2.1.1. European Union water legislation and reference documents

Water is a crucial resource for every living organism. It is also at the core of natural ecosystems and climate regulation. Therefore, in order to protect water, the European Parliament and Council introduced the Directive 2000/60/EC in 2000, also known as the EU Water Framework Directive (WFD) [5]. The WFD set out the basic principles for a sustainable water policy, and has been complemented by other legislation that regulates specific aspects of water use, as shown in Figure 2.1 [6].

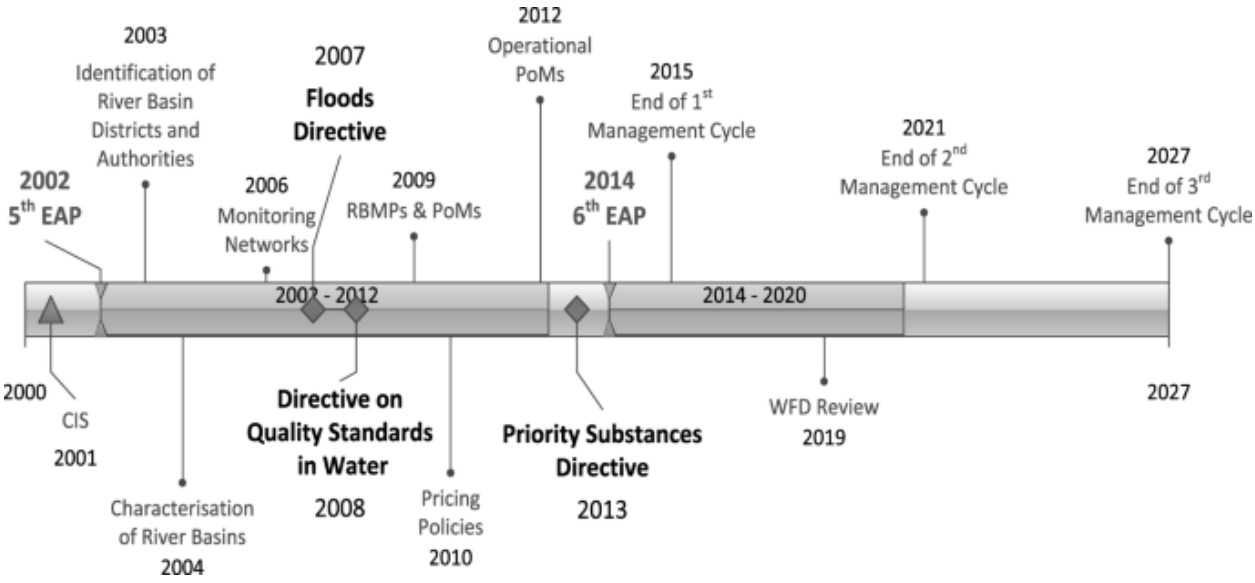


Figure 2.1. WFD implementation milestones and policy developments since its adoption (2000–2027) (EAP: Community Environmental Action Programmes). Reproduced from [7] under the terms of the Creative Commons CC BY license (https://creativecommons.org/licenses/).

In 2008, Directive 2008/105/EC identified 33 priority substances/classes (PSs) and their environmental quality standards (EQS). In 2013, Directives 2000/60/EC and 2008/105/EC were amended, and the most recent Directive 2013/39/EU includes a list of 45 PSs, highlighting the demand for innovative water treatment solutions and the importance of monitoring contaminants of emerging concern (CECs) for which legislation does not exist yet. According to the WFD, PSs pose "a significant risk to or via the aquatic environment" [2]. To name a few, PSs defined in Directive 2013/39/EU include: organochlorine pesticides (dieldrin, endosulfan), organophosphorus pesticides (chlorfenvinphos, chlorpyrifos), triazine pesticides (atrazine, simazine, terbutryn), phenylurea pesticides (diuron, isoproturon), chloroacetanilide pesticides (alachlor), dinitroaniline pesticides (trifluralin), PAHs (anthracene, naphthalene), alkylphenols (nonylphenol, octylphenol), perfluorinated compounds (*e.g.*, PFOS), phthalates (di(2-ethylhexyl) phthalate), solvents (1,2-dichloroethane, trichloromethane), dioxins and dioxin-like compounds, pyrethroid pesticides (cypermethrin), flame retardants (hexabromocyclododecanes), organotins (tributyltin) [2,8]. Contrarily, CECs include new

chemicals without regulatory status, which impact on the environment and human health is unknown [1] or not fully understood yet, and those that are currently detected using advances analytical techniques not available before. In this regard, the Decision 2015/495/EU has established a watch list of 10 CECs [9].

The watch list of Decision 2015/495/EU was updated by Decision 2018/840/EU and, more recently, by Decision 2020/1161/EU, specifying the CECs that should be monitored and considered for inclusion in the future regulatory revisions [9]. This current watch list of CECs includes: insecticide (metaflumizone), antibiotics (amoxicillin, ciprofloxacin, sulfamethoxazole, trimethoprim), antidepressant (venlafaxine and its metabolite o-desmethylvenlafaxine), azole compounds (clotrimazole, fluconazole, imazalil, ipconazole, metconazole, miconazole, penconazole, prochloraz, tebuconazole, tetraconazole), pesticide (dimoxystrobin) and fungicide (famoxadone) [10].

2.1.2. Origin, distribution, and fate

OMPs reach the environment through diverse sources. The most significant pollution pathways are the discharge of effluents from industrial, hospital and urban WWTPs that include the release of pharmaceuticals and cosmetic products; agriculture (mainly due to the pesticides); and livestock farming where veterinary drugs and food additives are used and excreted by animals and may reach the aquatic systems via runoff. A fraction of these pollutants can also infiltrate the soil after manure application and pollute the groundwater system. Leaching from dumping sites and sewage treatment facilities, as well as environmental disasters, are other possible sources [2].

The environmental fate of OMPs is mainly determined by the properties of the compound (chemical structure, octanol partition coefficient, acidity constant, among others) and by the conditions of the surrounding environment. Depending on these aspects, processes such as sorption, volatilization, dispersion, hydrolysis, oxidation, isomerization, photodegradation and biodegradation can occur [2]. As the environmental compartments are constantly interconnected, the occurrence of OMPs in surface water, ground water, soil and air can cause cumulative negative effects over multigenerational exposure in aquatic organisms and OMPs can even end up in drinking water [11].

2.1.3. Ecosystem and human health risks

There is still very limited information regarding the mid- and/or long-term effects of OMPs on ecosystems and human health, due to the complexity of environmental mixtures and the lack of multigenerational studies, among other factors. The continuous, but undetected effects of these OMPs may gradually accumulate, leading to irreversible changes. Therefore, it is

important to perform ecotoxicological risk or hazard assessments, which comprise the evaluation of the status and the changes that might occur in organisms due to their exposure to chemical contaminants and other possible stressors. Aquatic species have a higher risk of exposure; however, humans depend on the fate and behavior of OMPs in the surface and/or ground waters used to supply the drinking water treatment plants (DWTPs) [8,12].

It is known that PSs may remain in the environment for several years, are toxic for most organisms and can bioaccumulate, originating dermal toxicity, carcinogenicity, reproductive, neurological and developmental toxicity [8]. On the other hand, information on the impact of CECs is scarce, but it is speculated that they may have trophic consequences of multigenerational and population-level exposures, and thus the chronic effects over longer exposure periods that will affect the food chains should be consider [12].

2.2. Occurrence of pharmaceuticals in the environment

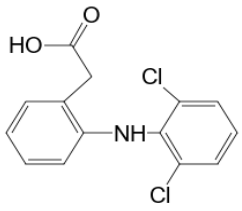
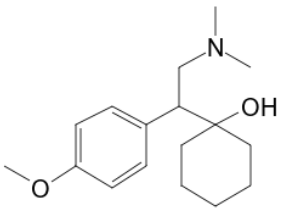
Pharmaceuticals have a significant importance in health care and life quality/expectancy. Worldwide, the yearly average consumption per capita is estimated to be about 15 g. In developed countries, its usage is even higher (50 to 150 g) [13]. A large amount of pharmaceuticals are used for the prevention, diagnosis and treatment of diseases in humans and other animals [13]. Due to the high levels of consumption of pharmaceuticals, there is a growing concern due to their recalcitrance upon degradation in conventional WWTPs, thus representing a continuous input into the environment [14,15].

Residues of pharmaceutical products may enter the environment during their manufacture, use and disposal. Consequently, their contribution for water pollution is an emerging problem, particularly in the case of antibiotics and the related generation of antimicrobial resistance [16]. Other classes of environmental concern include non-steroidal anti-inflammatory drugs (NSAIDs) and serotonin–norepinephrine reuptake inhibitors (SNRIs). Although concentrations of NSAIDs in waterways are relatively low, their high biological activity can pose a serious risk to non-target species at different levels of the ecological hierarchy, leading to different toxic effects [17]. Similarly, SNRIs have been detected at low concentrations in freshwater systems and in coastal waters, and studies have shown that they have adverse effects on non-target organisms [18,19]. Diclofenac (DCF) as a NSAIDs and venlafaxine (VFX) as a SNRIs were selected in this work due to their large consumption worldwide and their role as CECs commonly detected in aquatic environments [13,20,21]. In addition, VFX has recently been included in the watch list of CECs defined by Decision 2020/1161/EU [10].

As mentioned above, WWTPs do not effectively remove these drugs, since conventional treatments are not designed for this purpose. For instance, the rate of elimination of DCF and

VFX in conventional sewage treatment plants has been reported as being low (up to 40%) [20,22]. Their properties are summarized in Table 2.1. These drugs have a low hydrophobicity, as suggested by the octanol–water partitioning coefficients (log K_{ow}) and have a relatively low Henry's law constant. Thus, these compounds are less likely to volatilize in the atmosphere, which means that they tend to persist in water [23]. It is noteworthy that due to the polar nature of most pharmaceuticals, they are not significantly adsorbed in the subsoil and may leach into the groundwater aquifers [24]. Therefore, these polar target compounds have a likely affinity to the water phase, with VFX having a higher solubility in water than DCF. Consequently, it becomes extremely difficult to remove these compounds by the conventional treatments applied at WWTPs.

Table 2.1. Physicochemical and pharmacological properties of DCF and VFX [13,25-28].

	Diclofenac (DCF)	**Venlafaxine (VFX)**
Structure		
Molecular formula	$C_{14}H_{11}Cl_2NO_2$	$C_{17}H_{27}NO_2$
Molecular weight (*MW*)	296.149 g mol^{-1}	277.402 g mol^{-1}
CAS number	15307-86-5	93413-69-5
Usage	Analgesic, anti-inflammatory	Antidepressant
Water solubility	2.37 mg L^{-1} (25 °C)	267.0 mg L^{-1} (25 °C)
Henry's law constant	4.79×10^{-7} Pa m^3 mol^{-1} (25 °C)	2.04×10^{-6} Pa m^3 mol^{-1} (25 °C)
p*K*a	4.15	10.09
Log K_{ow}	4.51	3.20
Fluorescence wavelength	$\lambda_{exc.}$ = 285 nm $\lambda_{em.}$ = 360 nm	$\lambda_{exc.}$ = 230 nm $\lambda_{em.}$ = 300 nm
Dosage	75–150 mg d^{-1}	75–375 mg d^{-1}

2.2.1. Diclofenac

DCF (2-(2,6-dichlorophenylamino)phenyl acetic acid) is a NSAID prescribed either as pain reliever or to treat inflammatory conditions such as arthritic and rheumatic diseases [14,29]. Nowadays, this drug is ubiquitously detected in the aquatic ecosystems due to its recalcitrance to biodegradation [22]. Moreover, its occurrence is mainly due to the direct discharge of household, hospital, and pharmaceutical industrial wastewaters into the environment and/or the inefficiency of conventional WWTPs [22,30]. Although the ecotoxicity of DCF is relatively low, the toxic effect may increase considerably in combination with other drugs occurring in water reservoirs. Consequently, DCF might cause adverse effects to mammals, aquatic animals, plants, arthropods and earthworms, but also to humans after long-term exposure [29,30]. In order to gather representative monitoring data for this compound, Decision 2015/495/EU has determined that the maximum acceptable method detection limit for this NSAID should be 10 ng L^{-1} [31]. However, sufficient research data for this drug was gathered after the launch of Decision 2015/495/EU and as stated in Decision 2020/1161/EU [10], "the duration of a continuous monitoring period of the watch list for any individual substance shall not exceed four years", reason why DCF is no longer included in any watch list.

2.2.2. Venlafaxine

VFX (1-[2-dimethylamino-1-(4-methoxyphenyl)-ethyl]cyclohexanol) is an antidepressant that belongs to the class of SNRIs [21]. This antidepressant is widely used for the treatment of major depressive disorders, generalized anxiety disorder, panic disorder and social phobia [20,21].The occurrence of VFX in wastewater, and surface and drinking water is related to its low removal efficiencies in conventional WWTPs [32]. Consequently, the presence of VFX may induce chronic toxicity effects in the aquatic organisms [21]. Thereby, in order to gather representative monitoring data for this compound, Decision 2020/1161/EU has determined that the maximum acceptable method detection limit for this drug should be 6 ng L^{-1} [10].

2.3. Nanostructured carbon materials for adsorption

Recent studies on the use of carbon nanomaterials (NMs) as sorbents have been published, since these materials possess a high surface area-to-volume ratio that promises much greater adsorption capacity, as well as the possibility to easily modify their surface chemistry to improve the selectivity towards the target adsorbates [33].

Adsorption is a surface phenomenon in which the adsorbate is transferred from the aqueous phase onto the solid adsorbent [34]. Considering the water contamination concern, adsorption is considered one of the most adequate and applicable techniques due to its simplicity and easy

operation for pollutant removal. NMs can strongly adsorb many substances including trace metals and polar organic compounds [33,35]. The adsorption mechanisms include chemical adsorption, when covalent bonds are formed, or physical adsorption, when weak electrostatic interactions including London forces, Dipole-dipole forces, and Van der Waals interactions are established [34].

Hollow CSs have gained increasing interest for adsorption applications, especially because of their potential to store substances within their inner cavities. In order to confirm this hypothesis, different nanostructured CSs were synthetized in the present study, namely by adapting the procedure previously reported by Fuertes *et al.* [36], and these CSs were also employed in adsorption studies performed with DCF and VFX as model OMPs.

3. Materials and methods

3.1. Chemicals and instruments

Tetraethyl orthosilicate (TEOS; 99 wt.%), resorcinol (99 wt.%) and formaldehyde solution (37 wt.% in H_2O, containing 10-15% of methanol as stabilizer) were obtained from Sigma–Aldrich. Ammonia aqueous solution (28% v/v), sodium hydroxide and absolute ethanol (99.9 wt.%) were purchased from VWR. Diclofenac (sodium salt) and venlafaxine hydrochloride were purchased from Cayman and Supelco, respectively. Sodium chloride (99.5 wt.%) was purchased from JMGS. Acetonitrile and formic acid (99 wt.%) were purchased from VWR and used for high-performance liquid chromatography (HPLC). Distilled water was used for the synthesis of CSs, whereas ultrapure water supplied by a Milli-Q water system was used in all the other experiments.

The instruments used in this study were as follows: RADWAG AS 220.R2 analytical balance (± 0.0001 g) and Mettler PM2000 precision balance (± 0.01 g), Heraeus Instruments drying oven, Hitachi CT6E centrifuge (max. 4800 rpm), Shimadzu Corporation HPLC consisting of a Nexera X2 HPLC (chromatographic pump LC-30AD with a degasser DGU-20A 5R, an autosampler SIL-30AC, an oven CTO-20AC, a fluorescence RF-20A XS detector, and a system controller software), IKA® RCT basic safety control magnetic hotplate stirrer, IKA® WERKE RCT basic magnetic stirrer, oven, VWR pHenomenal® pH 1100L (± 0.1), TX4 digital vortex mixer by Velp® Scientifica with a IR Sensor, and other instruments for materials characterization descried in Section 3.3.

3.2. Synthesis of CSs

Silica@resorcinol–formaldehyde (SiO_2@RF) spheres were prepared by adapting the procedure described in the work of Fuertes *et al* [36]. Accordingly, 5 mL of ammonia aqueous solution (NH_4OH) was added to a mixture containing absolute ethanol (EtOH) and distilled water (H_2O) (ethanol/water volume ratios of 2, 4.5 and 7; considering a total volume of 160 mL), and then maintained at 30 ºC for 30 min under stirring (240 rpm). Subsequently, under vigorous stirring at 350 rpm, the following was added: (i) 5.6 mL of TEOS ($Si(OC_2H_5)_4$), which was stirred for 10 min; (ii) 0.8 g of resorcinol, which was stirred for 10 min; and finally, (iii) 1.12 mL of formaldehyde solution. The reaction mixture was then maintained at 30 ºC for 24 h under stirring (240 rpm), and at 100 ºC for 24 h under static conditions. Afterwards, the solid product was collected by centrifugation, washed with distilled water, and dried overnight at 100 ºC. The resulting material (SiO_2@RF spheres) was placed in a tubular vertical reactor with a porous plate and thermally annealed under a nitrogen flow (N_2, 100 cm^3 min^{-1}), at 3 sequential

temperature steps of 60 min each (120 ºC, 400 ºC and 600 ºC), followed by a period of 240 min at 800 ºC, with a heating rate set at 2 ºC min^{-1}. The carbonized product (SiO_2@CS) was treated in a strong basic solution of sodium hydroxide (NaOH, 10 mol L^{-1}) for 20 h at room temperature and under vigorous stirring to dissolve the silica core. The sample was washed with distilled water and collected by centrifugation, several times until the neutrality of the rinsing waters was reached, and then dried overnight at 100 ºC. The resulting materials were denoted as SiO_2@RF_X or CS_X, in which *X* represents the ethanol/water volume ratio used in the synthesis. The detailed synthesis parameters and other steps are given in Appendix A and Table A.1.

The thermal treatment under the inert atmosphere of N_2 allows the polymeric spheres to be directly converted into carbon spheres. Therefore, the weight-loss, *i.e.*, burn-off (*BO*) due to the thermal treatment, can be calculated as described in Eq. 1, where $m_{SiO_2@CS}$ (g) and $m_{SiO_2@RF}$ (g) represent the mass of SiO_2@CS and SiO_2@RF, respectively, for each ethanol/water volume ratio considered.

$$BO\ (\%) = \frac{m_{SiO_2@RF} - m_{SiO_2@CS}}{m_{SiO_2@RF}} \times 100 \quad (1)$$

3.3. Characterization techniques

The morphology of the CSs was studied by scanning electron microscopy (SEM), using a FEI Quanta 400 FEG ESEM/EDAX Genesis X4M apparatus coupled with energy-dispersive X-ray spectroscopy (EDS). SEM images were obtained in secondary electron (SE) and backscattered electron (BSE) detection modes, operating at 25 kV. The surface morphology was observed at different magnifications (from 100000 to 150000 times). ImageJ software was used to estimate the diameter of the CSs (at least 75 counts were performed for each material). The elemental composition of the CSs was studied by EDS.

Thermogravimetric analysis (TGA) was performed in a Netzsch STA 490 PC/4/H Luxx thermal analyzer, in which the sample (3 to 10 mg) was heated from 50 to 900 ºC at a rate of 10 ºC min^{-1}, under an oxidative (air) gas flow.

The textural characterization of the samples was based on adsorption-desorption isotherms of N_2 obtained at -196 ºC, which were performed in a Quantachrome Instruments, Nova 4200e Surface Area and Pore Size Analyzer apparatus equipped with a NovaWin™ software. Before the analysis, the samples (~ 0.1 g) were outgassed at a heating rate of 2 ºC min^{-1}, starting from 50 ºC until reaching 130 ºC, and then left under vacuum for 6 h. The specific surface area (S_{BET}) of the materials were calculated by the Brunauer–Emmett–Teller (BET) method using adsorption isotherms for relative pressures (P/P_0) between 0.05 and 0.30. The non-microporous surface area (S_{Meso}) and the volume of micropores (V_{Micro}) were calculated by the *t*-method using the

standard isotherms proposed by Thommes *et al.* [37]. The total pore volume (V_{Total}) was determined from the amount adsorbed at a relative pressure close to unity.

The pH at the point of zero charge (pH_{PZC}) of the materials was determined by pH drift tests, by adapting the procedure previously reported by Ribeiro *et al.* [38]. For that purpose, five sodium chloride (NaCl, 0.01 mol L^{-1}) solutions were prepared with different initial pH (2 – 11), as electrolyte. The preparation of the NaCl solutions is described in Appendix B. The samples (0.025 g) were then dispersed in these solutions, and the final pH measured after 64 h of continuous stirring at room temperature (23 ± 1 ºC). The pH_{PZC} was obtained considering the point where the experimental curve pH_{final} versus $pH_{initial}$ crosses the line $pH_{initial} = pH_{final}$. pH measurements were carried out with a pHenomenal® pH 1100L apparatus equipped with an SJ 223 pH electrode.

3.4. Kinetic and equilibrium adsorption experiments

Both adsorption kinetic and equilibrium studies were carried out at room temperature (23 ± 1 ºC), using a magnetic stirrer, and at the inherent pH of the distilled water (6.2 ± 0.1).

In kinetic adsorption experiments, a mass of CSs (5 mg) corresponding to a concentration of adsorbent (C_{ads}) of 0.25 g L^{-1} was added to a DCF or VFX solution with an initial concentration (C_0) of 100 mg L^{-1} (20 mL), in a 30 mL amber flask, and kept under stirring. Samples were filtered before analysis through 0.2 µm polytetrafluoroethylene (PTFE) syringe filters at predetermined intervals.

Equilibrium adsorption isotherm experiments were carried out in a MultiMix D MM90E Ovan to stir a constant mass of adsorbent (2.5 mg) dispersed in a constant volume of a DCF or VFX solution (10 mL) at various initial concentrations (ranging from 1 to 100 mg L^{-1}), keeping the ratio adsorbent mass/solution volume constant. Each amber flask was loaded and then sealed for the predetermined period needed to reach the equilibrium. Upon equilibrium, the samples were filtered and analyzed.

3.4.1. Modeling studies

The non-linearized forms of the kinetic and equilibrium adsorption models were fitted to the experimental data using the OriginLab software.

- **Kinetic modeling**

Kinetic aspects of adsorption processes are essential to understand the performance of the carbon materials. The adsorption models used by Álvarez-Torrellas *et al.* [39] were fitted to the

experimental data, in order to study the adsorption kinetic behavior of DCF or VFX onto the CSs.

The fractional power function model is an empirical model that describes the relation between the mass of the adsorbate per mass unit of the adsorbent and time "*t*". The non-linear expression is described in Eq. 2, where q_t (mg g^{-1}) is the adsorption capacity of DCF or VFX at a given time "*t*", and *a* (mg g^{-1} h^{-1}) and *b* are adjustment parameters.

$$q_t = a\, t^{\,b} \tag{2}$$

Lagergren pseudo-first order kinetic model has been used to describe the adsorption of different adsorbates from aqueous solution onto an adsorbent. The non-linear form is given in Eq. 3, where q_e (mg g^{-1}) is the equilibrium adsorption capacity and k_1 (h^{-1}) is the pseudo-first order rate constant.

$$q_t = q_e\,(1 - e^{-k_1\, t}) \tag{3}$$

The pseudo-second order model has been applied to the adsorption of metal ions, dyes, herbicides, oils, and organic substances from aqueous solutions. The non-linear form is presented by Eq. 4, where k_2 (g mg^{-1} h^{-1}) is the pseudo-second order adsorption rate constant.

$$q_t = \frac{q_e^2\, k_2\, t}{1 + q_e\, k_2\, t} \tag{4}$$

The Elovich model assumes that the active sites of the adsorbent are heterogeneous and therefore exhibit different activation energies for chemisorption. The non-linear form is shown in Eq. 5, where α (g mg^{-1} h^{-1}) is the initial adsorption rate and β (mg g^{-1} h^{-1}) is the desorption constant.

$$q_t = \beta \ln(\alpha \beta t) \tag{5}$$

- **Equilibrium modeling**

A dynamic equilibrium is established for solute distribution between the fluid and the solid surface. The most common approach to describe this equilibrium is to express the amount of solute adsorbed per amount of adsorbent as a function of the solute concentration in solution at constant temperature. This expression is called the adsorption isotherm [40].

The models used by Álvarez-Torrellas *et al*. allow to obtain valuable adsorption information, such as the adsorption mechanisms, the maximum adsorption capacity and the adsorbent properties from the adsorption isotherms [34].

The Langmuir and Freundlich models, which are both one-parameter isotherm models; and Sips, which is a three-parameter isotherm model, were fitted to the experimental data.

The assumptions underlying the Langmuir model are: (i) the distribution of adsorption sites is homogeneous; (ii) the adsorbate molecules are adsorbed onto the solid surface in a monolayer coverage without interaction between adsorbates; and (iii) the adsorbent surface is energetically uniform. The non-linear Langmuir model can be described by Eq. 6, where C_e (mg L^{-1}) is the equilibrium concentration of adsorbate in the solution, q_{sat} (mg g^{-1}) is a parameter that represents the maximum adsorption capacity in the monolayer and K_L (L mg^{-1}) is the Langmuir adsorption constant that is related to the adsorption energy and dependent on temperature.

$$q_e = \frac{q_{sat}\, K_L\, C_e}{1 + K_L\, C_e} \tag{6}$$

The Freundlich model is commonly used to describe heterogeneous surface energies. The Freundlich isotherm has the disadvantage of fitting well to the experimental data only over a range of moderate solute concentrations. The non-linear form of the Freundlich model is given by Eq. 7, where K_F (L^{1/n_F} mg^{1-1/n_F} g^{-1}) is the Freundlich constant and n_F is a parameter related to the adsorption intensity. The value of n_F reflects the degree of heterogeneity of the surface ($n_F > 1$ when the isotherm is favorable, $n_F < 1$ in the case of unfavorable isotherm and $n_F = 1$ when it is irreversible) [41].

$$q_e = K_F\, C_e^{\frac{1}{n_F}} \tag{7}$$

A combination of Langmuir and Freundlich isotherm models results in the Sips isotherm model. At low adsorbate concentrations, it reduces to Freundlich isotherm; while at high concentrations, it predicts a monolayer adsorption capacity characteristic of the Langmuir isotherm. Generally, the equation parameters are ruled mainly by the operating conditions such as the change of pH, temperature, and concentration. The non-linear form is presented by Eq. 8, where q_m (mg g^{-1}) is a parameter that represents the maximum adsorption capacity, K_s (L^{n_S} mg^{-n_S}) is the Sips isotherm model constant and n_S is a Sips parameter related to the heterogeneity of the adsorption system.

$$q_e = \frac{q_m\, (K_s\, C_e)^{\frac{1}{n_S}}}{1 + (K_s\, C_e)^{\frac{1}{n_S}}} \tag{8}$$

3.5. Analytical procedures

The determination of DCF or VFX concentrations was performed using a Shimadzu HPLC apparatus equipped with fluorescence detector. The separation was performed in a Kinetex™ XB-C18 100 Å column (100 × 2.1 mm, i.d.; particle diameter of 1.7 µm) and the optimized mobile phase consisted of 0.1% (v/v) formic acid and acetonitrile, at a flow rate of 0.25 mL min^{-1} and under gradient mode. Column oven and autosampler temperatures were set respectively at 30 and 15 ºC, and the volume of injection was 10 µL. Those samples whose concentration was above the range of the calibration curves were diluted in ultrapure water and the dilution factor was considered for the estimation of the concentrations in the samples. Appendix C details the procedure and the results obtained for the calibration curves that were used to determine the concentrations of the solutions; shows the chromatographic separation of DCF and VFX, with the respective retention time (Figure C.1); details the correlation coefficient and limits of detection and quantification (Table C.1); and, lastly, the study of the precision of the analytical procedure used (Tables C.2 to C.3).

4. Results and discussion

4.1. Mechanistic insights into the synthesis of CSs

The CSs were obtained by adapting the procedure reported by Fuertes *et al.*, namely the one-step synthesis of silica@resorcinol-formaldehyde (SiO_2@RF) spheres based on Stöber's conditions [36]. The Stöber's method is a pioneering approach for the synthesis of spherical and monodisperse silica nanoparticles of uniform size by hydrolysis and condensation of silicon alkoxides (*i.e.*, TEOS) in an ethanol/water (E/W) mixture, and in the presence of ammonia as a catalyst [42]. Briefly, the synthesis of SiO_2@RF in a single step was possible since SiO_2 particles were formed first (higher reaction rate), and only then covered with resorcinol and formaldehyde (24 h at 30 ºC), which finally undergo a complete sol-gel polycondensation reaction at 100 ºC.

Three chemical reactions are generically used to describe the hydrolysis and condensation reactions of silicon alkoxides, as described by Eqs. 9-11 [43], where R represents an alkyl group C_xH_{2x+1}. In the hydrolysis reaction described by Eq. 9, the alkoxide groups (—OR) are replaced by hydroxyl groups (—OH). Condensation reactions yield siloxane bonds and either alcohol (ROH) or water (H_2O), as described by Eqs. 10 and 11, respectively.

$$\equiv\text{Si-OR} + H_2O \overset{\text{hydrolysis}}{\rightleftharpoons} \equiv\text{Si-OH} + \text{ROH} \quad (9)$$

$$\equiv\text{Si-OR} + \equiv\text{Si-OH} \overset{\text{alcohol condensation}}{\rightleftharpoons} \equiv\text{Si-O-Si} + \text{ROH} \quad (10)$$

$$\equiv\text{Si-OH} + \equiv\text{Si-OH} \overset{\text{water condensation}}{\rightleftharpoons} \equiv\text{Si-O-Si} + H_2O \quad (11)$$

Bogust *et al.* [43] mentioned that in general, the reactions described by Eqs 9-11 are reversible. Since the water and silicon alkoxides are immiscible, a mutual solvent such as alcohol is usually used as a homogenizing agent [44] affecting the monodispersity of the silica particles [45].

Because this reaction occurs is an alcoholic solution, *i.e.*, it is performed under basic conditions, the water dissociates to produce hydroxyl anions (HO^-) [44,46], in that way the hydrolysis reaction is initiated by the attack of HO^- on TEOS molecules. When an ethoxy group is replaced by a hydroxyl group, the electron density of silicon is reduced, accelerating the hydrolysis rate of another —OR. Once an —OR is hydrolyzed, the others will be hydrolyzed rapidly, followed by the condensation of $Si(OH)_4$, resulting in the formation of silica spheres, known as silica Stöber spheres. Accordingly, the —OH of $Si(OH)_4$ reacts with either the —OR of another TEOS, through the "alcohol condensation" reaction as described by Eq. 10, or with an —OH intermediate of another hydrolysis, through the "water condensation" reaction as

described by Eq. 11, to form Si-O-Si bridges. Kim *et al*. mentioned that the rate of water condensation is over 1000-fold higher than that of the alcohol condensation reaction [47].

According to the literature, five parameters can influence the size (and size distribution) of spherical SiO_2 particles: (i) concentration of ammonia, (ii) concentration of TEOS, (iii) alcohol/water ratio, (iv) type of alcohol, and (v) temperature [42,43,45,46,48].

Fuertes *et al*. found that silica spheres are efficiently produced when employing E/W volumetric ratios equal or above 2 [36], whereas 7 was the highest E/W ratio used by Stöber *et al*. [42]. Therefore, in this study, the E/W ratio ranged between 2 and 7. Fuertes *et al*. reported that the E/W ratio was the parameter that most influences the size of the resulting SiO_2 particles [36]. Therefore, the effect of the E/W ratio on the particle size was studied in the present work. In this sense, by adjusting the E/W ratio used in the synthesis, materials with varying diameters were expected to be obtained, and thus the influence of particle size of hollow CSs on the adsorption of DCF and VFX could be studied for the first time.

The presence of ammonia is known to influence the morphology of the resulting particles, leading to materials with spherical shape [42]. Moreover, ammonia accelerates the polymerization of resorcinol with formaldehyde and provides positive charges that adhere to the outer surface of the spheres, thus preventing aggregation [48,49].

Once (i) SiO_2 spheres were obtained, the subsequent steps involved in the synthesis of hollow CSs were those depicted in Figure 4.1, namely (ii) polymerization of resorcinol (R) with formaldehyde (F), (iii) carbonization, and (iv) etching of the SiO_2 core.

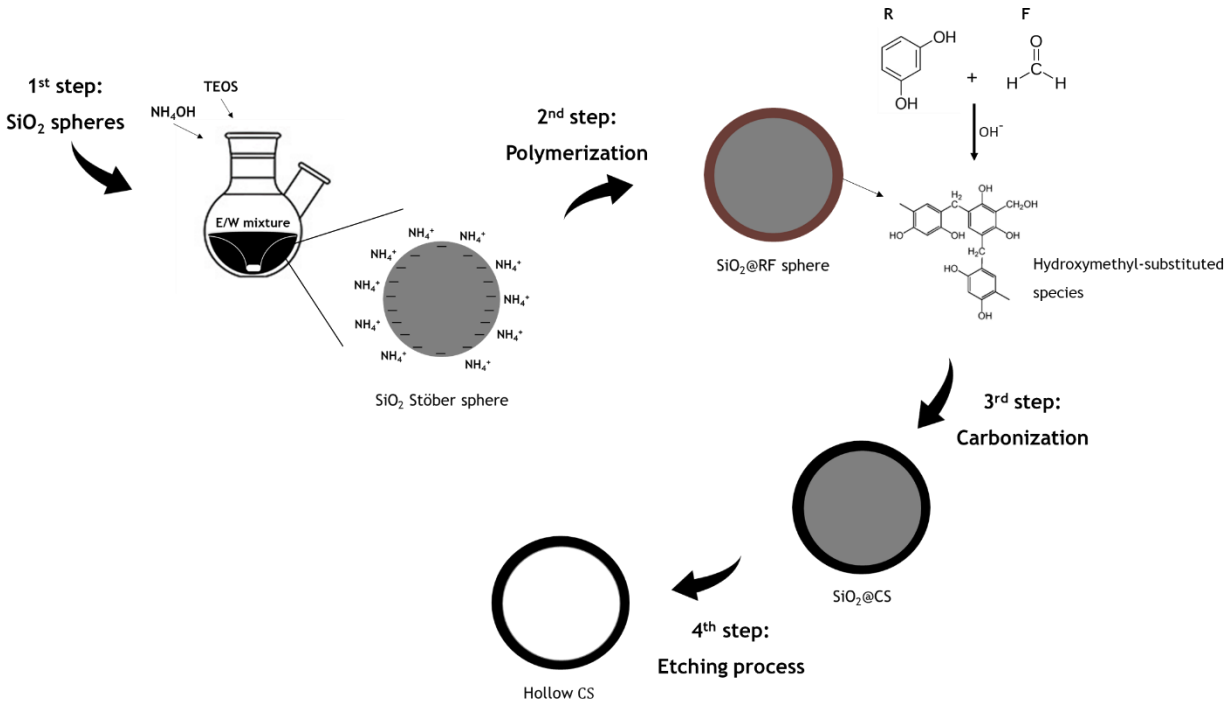


Figure 4.1. Schematic representation of the synthesis of hollow CSs.

The formation of SiO_2 spheres occurs during the first stage of the synthesis procedure. These are quickly obtained after addition of TEOS to an aqueous solution containing ethanol and NH_4OH. As can be seen in Figure 4.2, a turbid white suspension started being formed about 10 min after TEOS was added. This suggests the formation of a stable colloidal suspension of SiO_2 (*i.e.*, particle aggregation and/or sedimentation is negligible) due to the use of the aqueous ammonia solution, as mentioned earlier. The NH_4^+ ions cover the surface of the silica particles, which are negatively charged. The second step (polymerization) was then initiated when both resorcinol and formaldehyde were added to the SiO_2 suspension. Resorcinol reacts with formaldehyde to form numerous hydroxymethyl-substituted (HS) species. This reaction (catalyzed by HO^- ions) is much slower than the Stöber reaction and requires higher temperature to be completed (up to 100 ºC). Once formed, the HS species will gradually diffuse to the surface of the SiO_2 particles due to electrostatic interactions with the NH_4^+ ions attached to its surface, resulting in the formation of a first RF polymeric layer around the SiO_2 spheres. SiO_2@RF spheres with a core@shell structure were obtained as the polymerization reaction proceeded for 24 h at 30 ºC, and then 24 h at 100 ºC. Accordingly, a remarkable change in the solution color was observed during the polymerization step. As shown in Figure 4.2, the turbid white suspension of SiO_2 gradually became dark reddish-brown as SiO_2@RF spheres were formed.

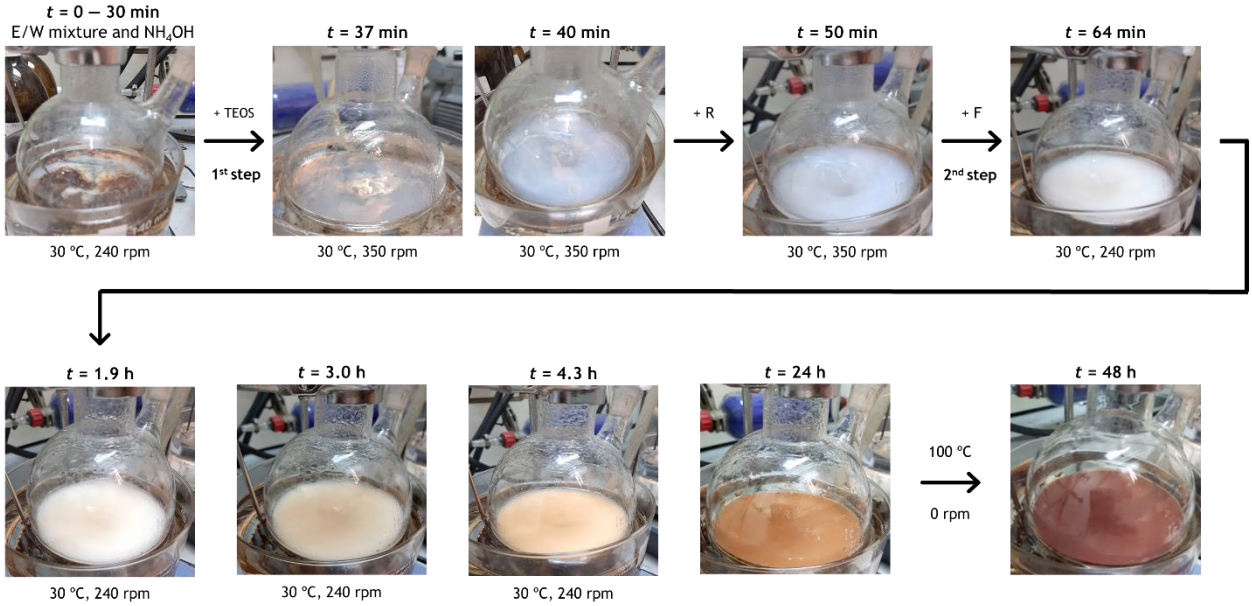


Figure 4.2. Pictures taken during the synthesis of SiO_2@RF spheres.

The third step of the synthesis of the CSs took place upon thermal annealing of the SiO_2@RF spheres at 800 ºC under N_2 atmosphere. During this step, the RF polymeric layer was carbonized while the SiO_2 core was unaffected. Figure 4.3 shows the material before (SiO_2@RF spheres) and after (SiO_2@CS) carbonization. It is worth mentioning that all the materials produced

(*i.e.*, with different E/W ratios) undergone thermal annealing with N_2 flow and it was possible to observe a color change from reddish-brown to black in all of them.

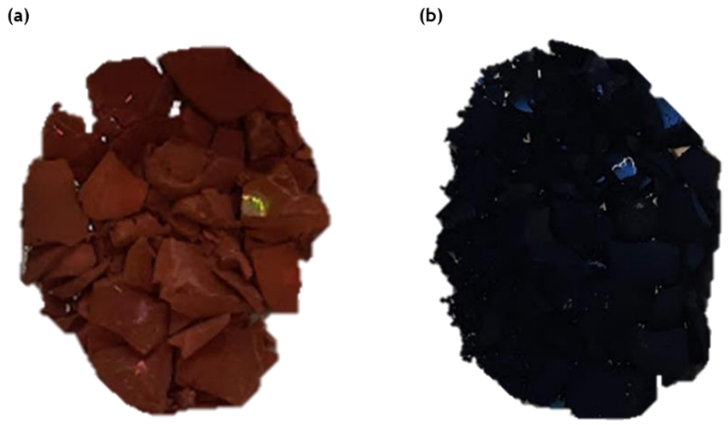


Figure 4.3. Pictures of (a) SiO_2@RF and (b) SiO_2@CSs.

In the fourth and last step, the SiO_2 core of the carbonized product (SiO_2@CS) was removed by an etching process in a strong basic NaOH solution, as described in Appendix A. A fraction of the carbonized product was kept with the silica core (without etching) and stored for further use.

4.2. Characterization of CSs

4.2.1. Scanning electron microscopy

SEM analysis was used to study the morphology, particle size and size distribution, and aggregation/dispersion of the synthesized materials. As observed in the SEM images given in Figure 4.4, all the materials exhibited a spherical morphology, and the particles were dispersed. It is also visible that the final hollow core, within the CSs, had a regular and smooth surface (Figure 4.4d and f), except for CS_2 (Figure 4.4b), in which a partial rupture of the spherical carbon shell apparently occurred during the etching process (*i.e.*, when testing the lower E/W volumetric ratio).

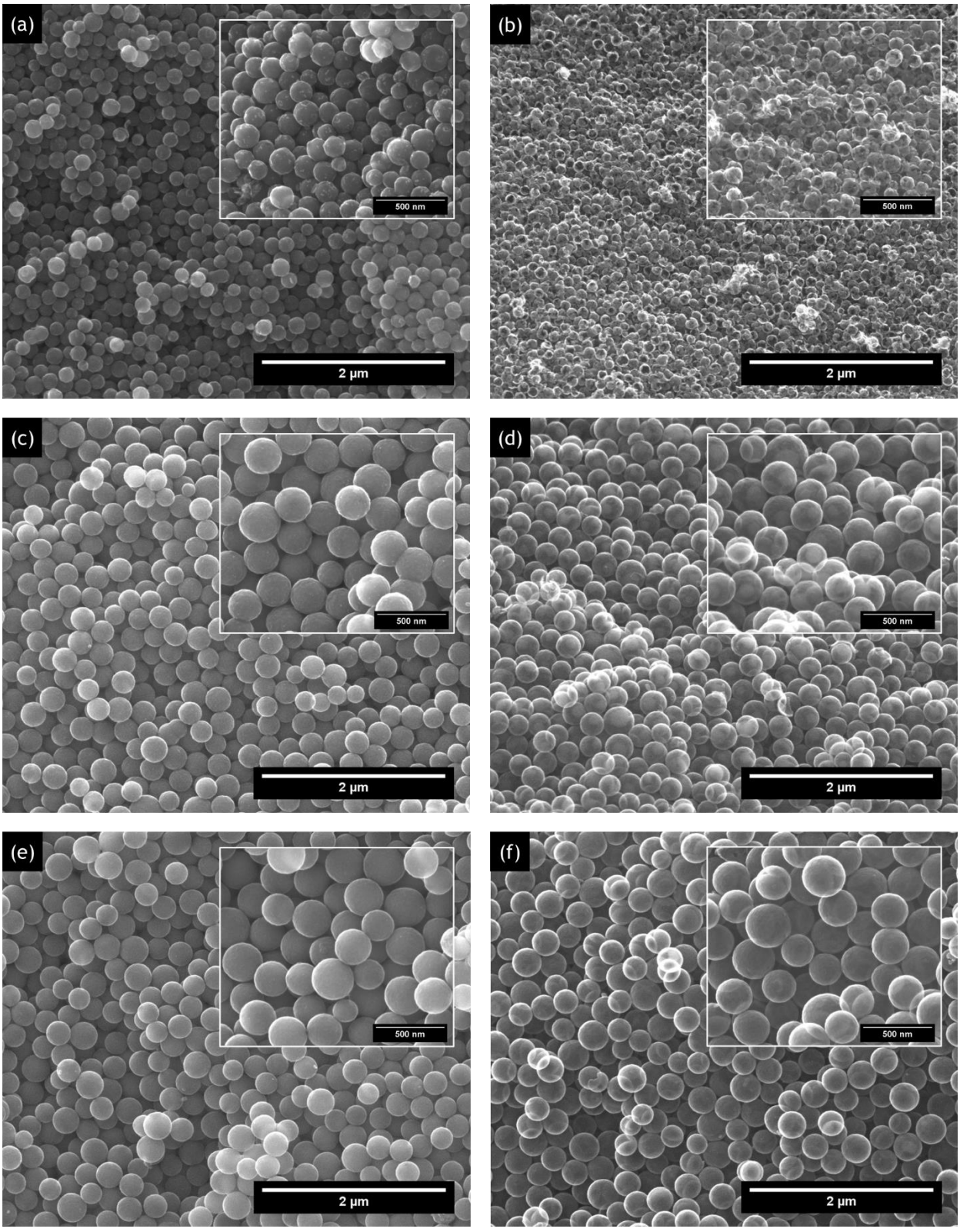


Figure 4.4. SEM micrographs of: (a) $SiO_2@CS_2$, (b) CS_2, (c) $SiO_2@CS_{4.5}$, (d) $CS_{4.5}$, (e) $SiO_2@CS_7$, and (f) CS_7. Images obtained in SE mode.

Table 4.1 and Figure 4.5 show the average diameter ($d_{average}$) of the CSs, as determined by SEM measurements, and the associated standard deviations. The histograms of particle size distribution are shown in Appendix B (Figure B.1). As expected, $d_{average}$ increased with the E/W ratios. Moreover, the $d_{average}$ before and after the SiO_2 dissolution step suggests that the CSs

prepared with an E/W ratio of 2 had slightly shrunk during this process, *i.e.*, there was a decrease of the $d_{average}$ of SiO_2@CS_2 upon etching with NaOH, corresponding to around 54% of its initial size. As for the materials prepared with E/W ratios of 4.5 and 7, the $d_{average}$ are negligibly affected by the etching of the SiO_2 core, as can be seen in Figure 4.5. This suggests that the CSs became more resistant to the etching process by increasing E/W ratios. However, the silica removal in $CS_{4.5}$ and CS_7 was not as effective as with CS_2 (see Section 4.2.2), which may also influence the particle diameter.

Table 4.1. Average diameters ($d_{average}$) of the tested materials and their associated standard deviations.

Sample	SiO_2@CS_2	CS_2	SiO_2@$CS_{4.5}$	$CS_{4.5}$	SiO_2@CS_7	CS_7
$d_{average}$ / nm	168 ± 21	109 ± 13	251 ± 24	245 ± 25	270 ± 26	284 ± 32

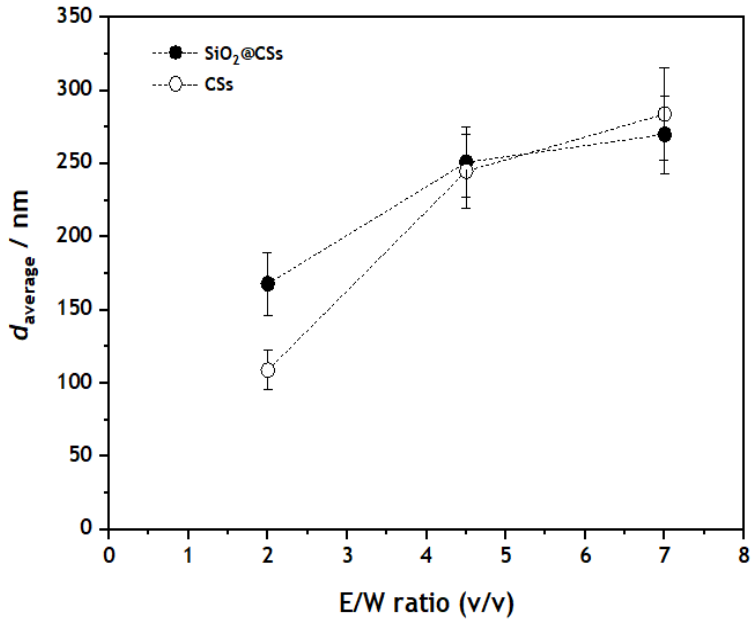


Figure 4.5. Particle diameter of SiO_2@CSs and CSs as a function of the E/W ratio.

After the SiO_2 dissolution step, some transparencies were observed in the SEM micrographs (Figure 4.4), *i.e.*, some CSs in the background can be observed through the outline of the carbon shell of CSs in the foreground. This feature is particularly visible for $CS_{4.5}$ and CS_7 (insets of Figure 4.4d and f, respectively), suggesting that the dense SiO_2 cores were effectively removed upon dissolution with NaOH. Bearing this in mind, additional SEM micrographs were obtained in BSE mode (Figure 4.6). Under this detection mode, denser chemical elements were recorded as brighter regions, thus allowing to distinguish carbon from silica. Accordingly, only large bright spheres are observed in the SEM micrographs of SiO_2@CS_2, SiO_2@$CS_{4.5}$ and SiO_2@CS_7 (Figure 4.6a, c, and e, respectively), which correspond to the SiO_2 cores. On the contrary, almost no bright zones were found in the SEM micrographs of CS_2 and CS_7 (Figure 4.6b and f,

respectively), confirming the effectiveness of the silica etching process. However, some small bright spheres were still found in the SEM micrograph of $CS_{4.5}$ (Figure 4.6d), showing that the etching process was not so effective in this case.

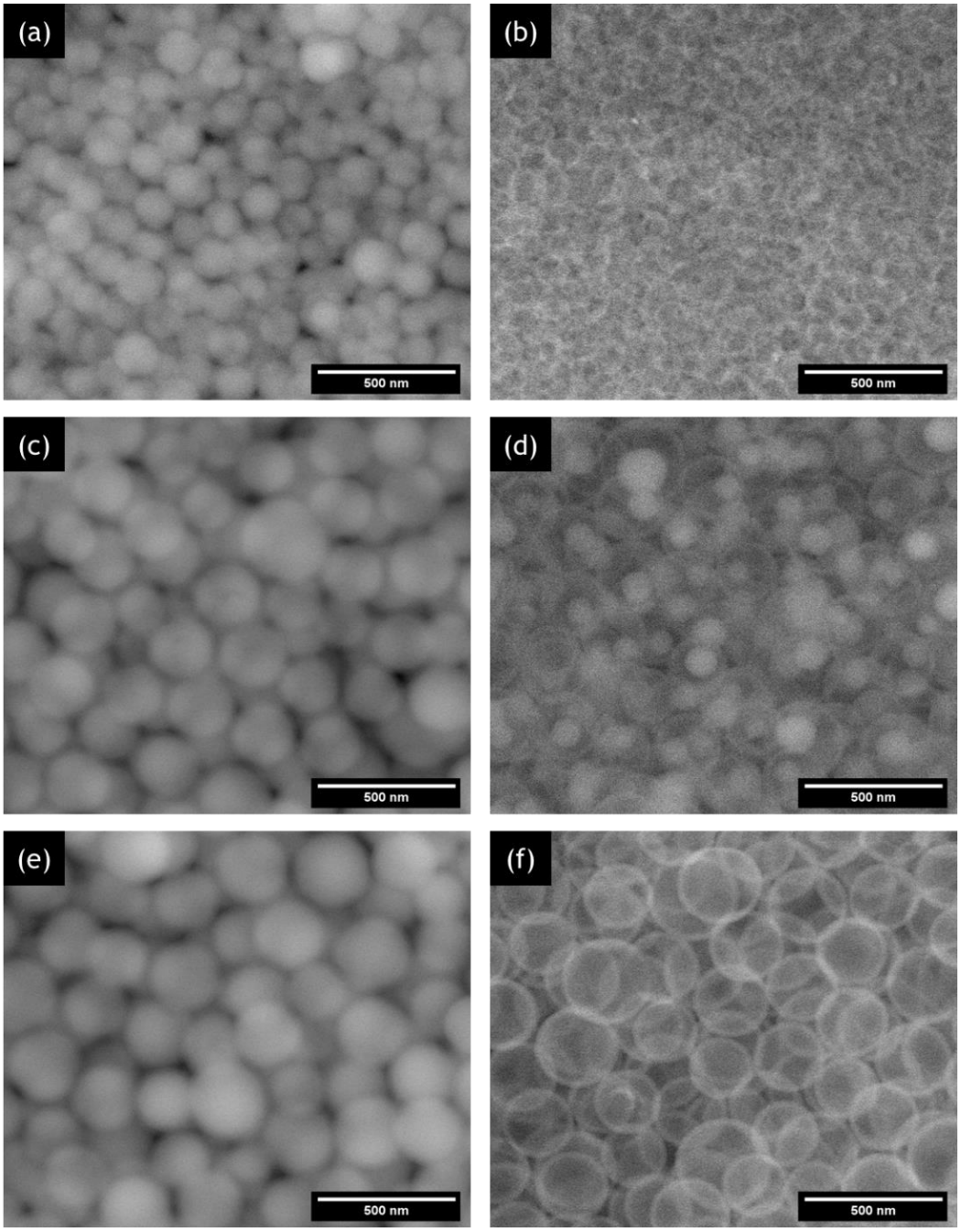


Figure 4.6. SEM micrographs of: (a) $SiO_2@CS_2$, (b) CS_2, (c) $SiO_2@CS_{4.5}$, (d) $CS_{4.5}$, (e) $SiO_2@CS_7$, and (f) CS_7. Images obtained in BSE mode.

The previous observations on the effectiveness of the silica removal step were also studied by EDS. As observed in Figure 4.7, the predominant element in the spectra of $SiO_2@CS_2$, $SiO_2@CS_{4.5}$ and $SiO_2@CS_7$ was silicon, whereas carbon was predominant in the spectra of CS_2, $CS_{4.5}$ and CS_7. Nevertheless, some silicon was still present in $CS_{4.5}$ and CS_7, which is in agreement with the previous SEM observations. In addition, this elemental mapping analysis only shows trace

amounts of the element sodium ($CS_{4.5}$ and CS_7), indicating that the washing step after the etching process was successful as well.

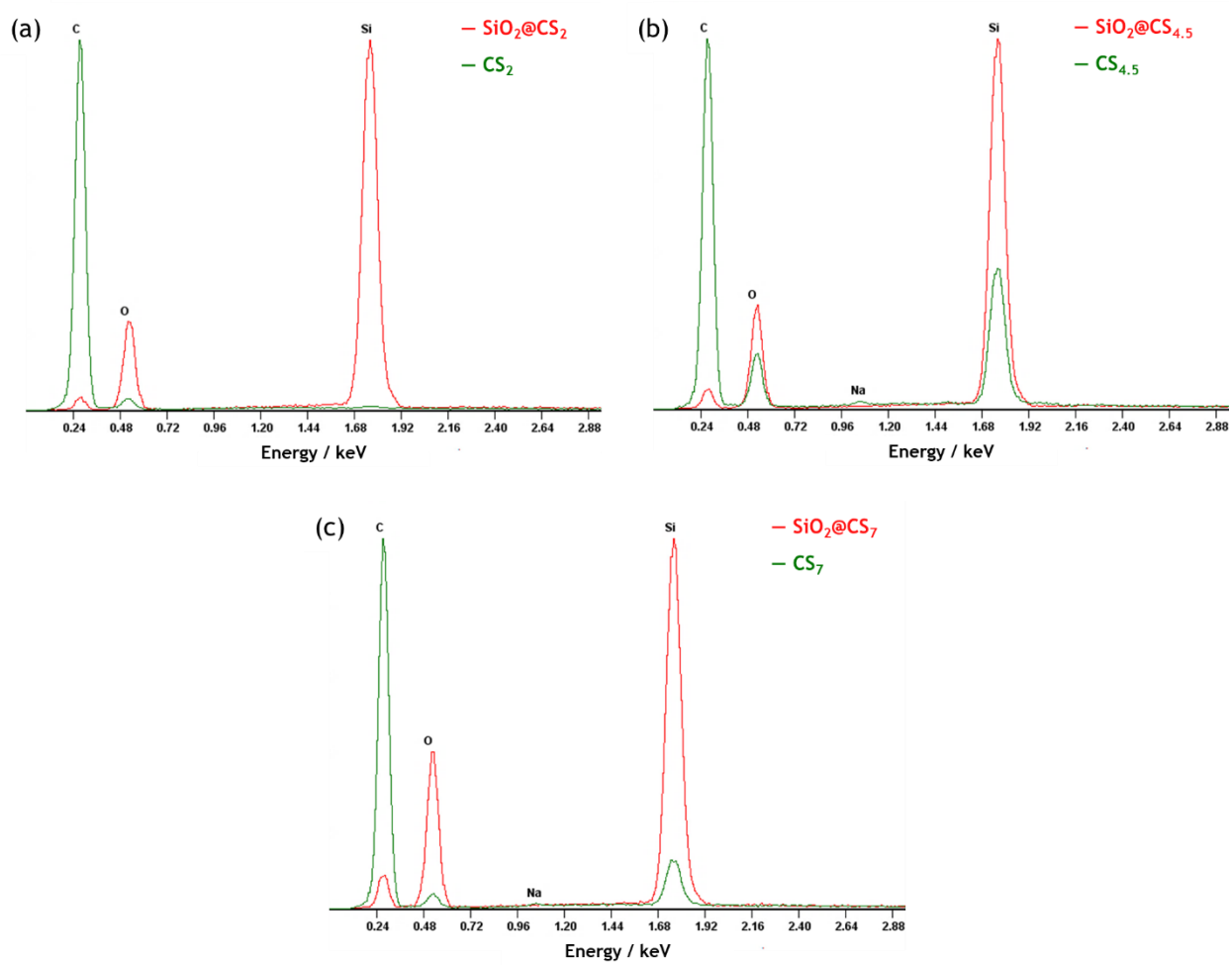


Figure 4.7. EDS spectra of: (a) $SiO_2@CS_2$ and CS_2, (b) $SiO_2@CS_{4.5}$ and $CS_{4.5}$ and (c) $SiO_2@CS_7$ and CS_7. Data obtained over a global area of each sample.

4.2.2. Thermogravimetric analysis

TGA under oxidative atmosphere was used to quantify the silica content in the CSs, and thus better elucidate the results obtained by SEM-EDS on the effectiveness of the silica removal using the NaOH solution. The corresponding TGA curves are given in Figure 4.8 and the TGA residues summarized in Table 4.2. As observed, all the $SiO_2@CSs$ have a high ash content (TGA residue ranging from 76 to 81 wt.%), which can be ascribed to the SiO_2 core. On the contrary, CS_2 revealed a negligible ash content (3 wt.%), confirming that the treatment with NaOH successfully removed the SiO_2 core from this material. CS_7 revealed an ash content of 24 wt.%, whereas $CS_{4.5}$ revealed a higher amount (46 wt.%). These results agree with those previously obtained by SEM-EDS, allowing to conclude that the etching process was more effective in the case of CS_2, followed by CS_7; and not as effective in the case of $CS_{4.5}$.

Figure 4.8 also provides the first derivate of the TGA curve (DTGA) information. As observed, the weight loss was more pronounced at around 600 ºC for all the materials, which can be attributed to the oxidation of the carbon phase. Indeed, the carbon content of the materials can be estimated as the mass fraction not corresponding to ashes. The results obtained are also given in Table 4.2.

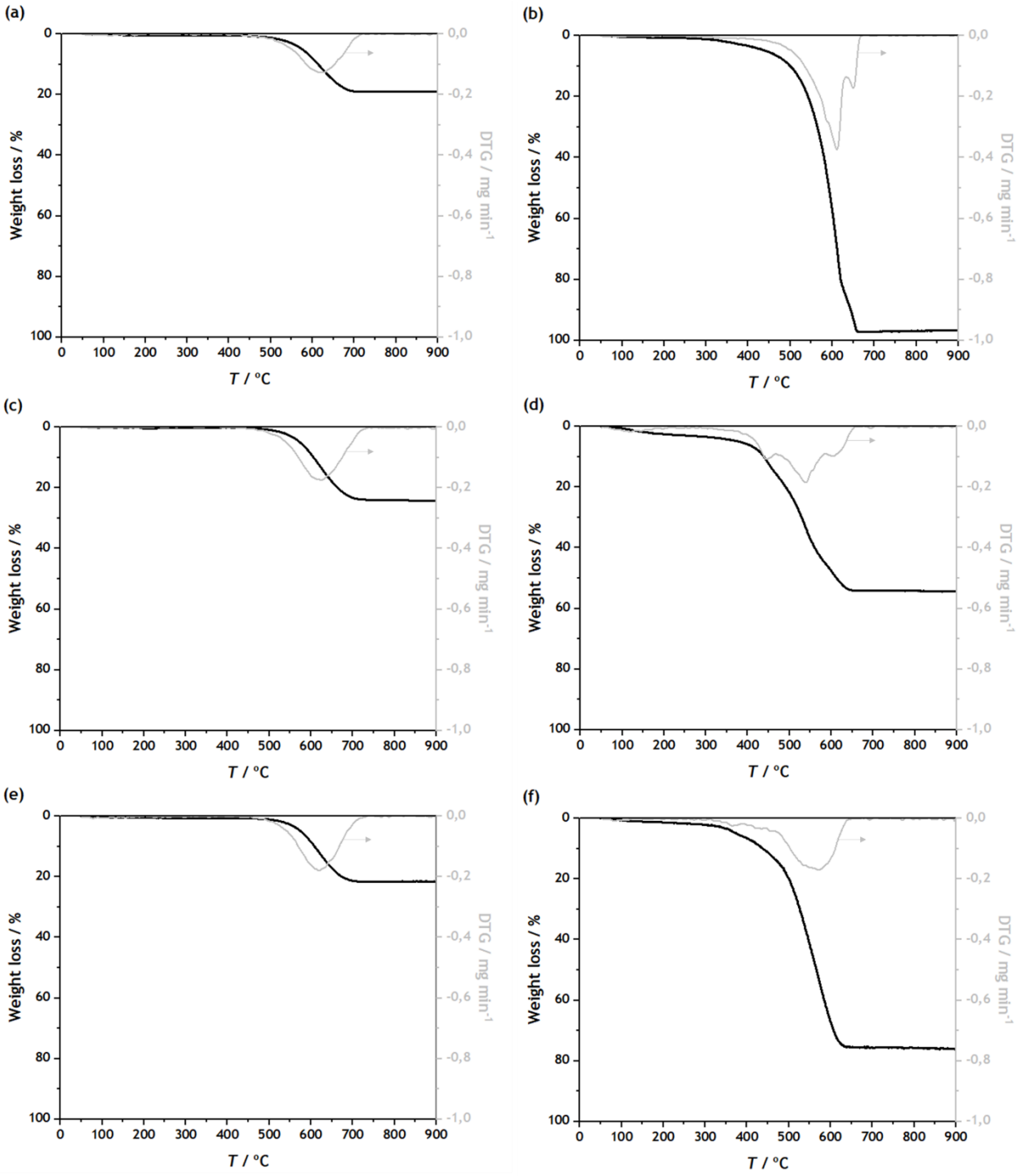


Figure 4.8. TGA and DTGA curves in oxidative (air) atmosphere: (a) $SiO_2@CS_2$, (b) CS_2, (c) $SiO_2@CS_{4.5}$, (d) $CS_{4.5}$, (e) $SiO_2@CS_7$ and (f) CS_7.

Table 4.2. TGA residues and carbon content of the CSs, as determined by TGA under air atmosphere.

Sample	TGA Residue / wt.%	Carbon content [a] / wt.%
SiO_2@CS_2	81	19
CS_2	3	97
SiO_2@$CS_{4.5}$	76	24
$CS_{4.5}$	46	54
SiO_2@CS_7	78	22
CS_7	24	76

[a] Estimated as the mass fraction not corresponding to ashes (TGA residue).

4.2.3. Textural characterization

The N_2 adsorption–desorption isotherms obtained with the synthesized materials are shown in Appendix B (Figure B.2), and their main textural properties summarized in Table 4.3. As observed, all the materials possessed both micropores (as indicated by the adsorption of N_2 at low relative pressures) and mesopores (as indicated by the adsorption of N_2 at high relative pressures, as shown in Figure B.2). Nevertheless, the porosity of the SiO_2@CSs is always lower than that of the corresponding hollow CSs. This trend becomes clearly visible when the textural properties given in Table 4.3 are compared and can be explained by the higher content of less porous silica (S_{BET} ≈ 20 m^2 g^{-1}, as determined elsewhere [50]) in the SiO_2@CSs (as discussed in Sections 4.2.1 and 4.2.2). For instance, the specific surface area (S_{BET}) of the SiO_2@CSs ranged from 115 to 144 m^2 g^{-1}, while the S_{BET} of the CSs ranged from 271 to 602 m^2 g^{-1}.

A closer look at the CSs obtained with an E/W volumetric ratio of 2 allows further highlighting the effect of silica etching on the textural properties of the materials. As determined by TGA, the estimated carbon content of SiO_2@CS_2 is 19 wt.%, which is 5.1-fold lower than that of CS_2 (97 wt.%, as given in Table 4.2). At the same time, the S_{BET} of SiO_2@CS_2 (115 m^2 g^{-1}) is 4.7-fold lower than that of CS_2 (545 m^2 g^{-1}, as given in Table 4.3), and the mesoporous surface area (S_{Meso}) is 4.9-fold lower. These observations suggest that the textural properties of the carbon phase are negligibly affected by the etching process with NaOH, as the increase of the surface area can be explained by the removal of silica. Regarding the pore volume, two different trends can be observed. On the one hand, the micropore volume (V_{Micro}; corresponding to pores < 2 nm) increases 4.6-fold upon removing the silica core (from 0.023 cm^3 g^{-1} in SiO_2@CS_2, to 0.105 cm^3 g^{-1} in CS_2, as given in Table 4.3), which can be explained as discussed above for the surface area. On the other hand, the total pore volume (V_{Total}) of CS_2 (1.912 cm^3 g^{-1}) is 6.3-fold higher than that of SiO_2@CS_2 (0.305 cm^3 g^{-1}, as given in Table 4.3), suggesting a contribution of the hollow core towards the porosity (pores > 2 nm) of CS_2. Similar trends are observed for the CSs prepared with E/W volumetric ratios of 4.5 and 7. Briefly, the S_{BET} of $CS_{4.5}$ (271 m^2 g^{-1}) is

2-fold higher than that of $SiO_2@CS_{4.5}$ (137 $m^2\ g^{-1}$), while the estimated carbon content of $CS_{4.5}$ is 2.3-fold higher than that of $SiO_2@CS_{4.5}$; and the S_{BET} of CS_7 (602 $m^2\ g^{-1}$) is 4.2-fold higher than that of $SiO_2@CS_7$ (144 $m^2\ g^{-1}$), while the estimated carbon content of CS_7 is 3.5-fold higher than that of $SiO_2@CS_7$. Moreover, a contribution of the hollow cores towards porosity is also suggested in these cases, as the V_{Total} of the materials prepared with E/W volumetric ratios of 4.5 and 7 increase 6 and 10.8-fold upon etching the silica cores, respectively.

Table 4.3. Specific surface area (S_{BET}), non-microporous surface area (S_{Meso}), micropore volume (V_{Micro}) and total pore volume (V_{Total}) of the CSs.

Sample	S_{BET} / $m^2\ g^{-1}$	S_{Meso} / $m^2\ g^{-1}$	V_{Micro} / $cm^3\ g^{-1}$	V_{Total} / $cm^3\ g^{-1}$
$SiO_2@CS_2$	115	59	0.023	0.305
CS_2	545	288	0.105	1.912
$SiO_2@CS_{4.5}$	137	57	0.033	0.159
$CS_{4.5}$	271	122	0.065	0.960
$SiO_2@CS_7$	144	43	0.042	0.143
CS_7	602	392	0.083	1.548

4.2.4. Surface chemistry characterization

The surface chemistry of the carbon materials was broadly characterized by the determination of pH_{PZC}. According to the literature [51], the pH_{PZC} is defined as the pH at which the overall surface charge of a given material is null. The surface charge is negative at pH > pH_{PZC} and positive at pH < pH_{PZC}. This will be important to explain some of the results obtained in the adsorption experiments. The results obtained in the pH drift tests performed to determine the pH_{PZC} are shown in Appendix B (Figure B.3) and summarized in Table 4.4. As observed, all the CSs possess a basic nature ($pH_{PZC} \geq 7.9$), although this character is more pronounced in the case of $CS_{4.5}$ and CS_7 ($pH_{PZC} \approx 10$).

Table 4.4. pH at the point of zero charge (pH_{PZC}) data of the CSs.

Sample	CS_2	$CS_{4.5}$	CS_7
pH_{PZC}	7.9 ± 0.1	10.0 ± 0.1	10.1 ± 0.1

4.3. Kinetic adsorption experiments

Kinetic adsorption experiments were conducted with two main objectives, namely to (i) determine the time needed to reach the adsorption equilibrium (to be used in the adsorption equilibrium experiments discussed in Section 4.4), and (ii) study the effect of the hollow core of the CSs on the adsorption performance. The material prepared with the E/W volumetric ratio of 2 was selected for the kinetic study herein reported.

Two preliminary experiments were carried out with $SiO_2@CS_2$ and CS_2 for 96 h (data not shown). In the case of $SiO_2@CS_2$, the adsorption capacity for both DCF and VFX was negligible during the whole assays (data not shown). On the other hand, the time needed for the adsorption equilibrium to be reached in the case of CS_2 was below 24 h regardless of the OMP considered. Thus, the following experiments were performed for 24 h, including experiments performed in triplicate with CS_2 (Figure 4.9). The detailed kinetic data is detailed in Appendix D (Table D.1). As observed, the adsorption capacity at a given time (q_t) reached a plateau at around 4 to 6 h, both in the case of DCF and VFX, confirming that the adsorption equilibrium was reached under these conditions. Moreover, kinetic modelling was performed as described in Section 3.4.1. Table 4.5 shows all the parameters related to the kinetic models applied, as well as the corresponding correlation coefficients (r^2). Considering the r^2 values, it can be observed that all the models could reasonably fit to the experimental data. Among the models studied, namely fractional power, pseudo-first order, pseudo-second order, and Elovich models (Eqs. 2-5), the pseudo-first order model was found to be the most suitable for fitting the experimental DCF kinetic data and the fractional power model to VFX adsorption data. Therefore, the curves obtained with these models are shown in Figure 4.9.

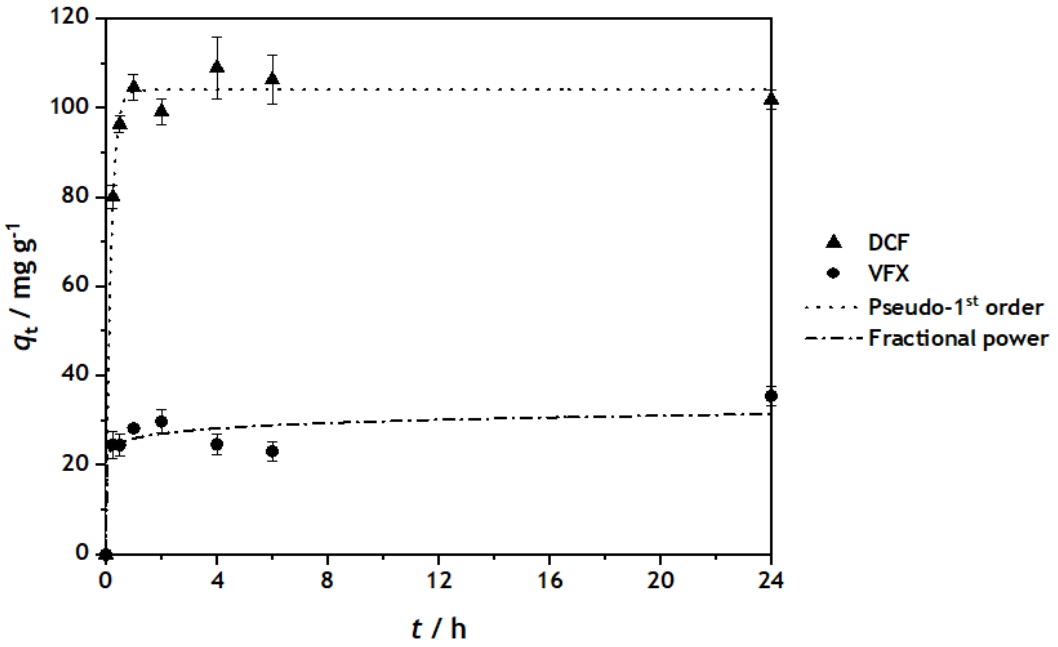


Figure 4.9. Kinetic experimental and theoretical data for the adsorption of DCF and VFX onto CS_2. Experiments performed with $[CS_2]$ = 0.25 g L^{-1}, $[DCF]_0$ or $[VFX]_0$ = 100 mg L^{-1}, pH = 6.4 or 6.2 (inherent pH of DCF and VFX solutions, respectively), T = 23 ± 1 °C (room temperature), and stirring speed of 200 rpm.

Table 4.5. Kinetic model parameters (non-linearized form equations) for the adsorption of DCF and VFX onto CS_2.

Fractional power model	a / mg g^{-1} h^{-1}	b	r^2
DCF	96.79	0.04	0.9661
VFX	26.02	0.06	0.9000
Lagergren pseudo-first order model	q_e / mg g^{-1}	k_1 / h^{-1}	r^2
DCF	104.13	5.74	0.9932
VFX	27.91	7.73	0.8646
Pseudo-second order model	q_e / mg g^{-1}	k_2 / g mg^{-1} h^{-1}	r^2
DCF	107.13	0.13	0.9897
VFX	28.72	0.68	0.8738
Elovich model	α / g mg^{-1} h^{-1}	β / mg g^{-1} h^{-1}	r^2
DCF	2.37 × 10^9	4.20	0.9676
VFX	1.24 × 10^7	1.56	0.8973

It is also observed in Figure 4.9 that the adsorption capacity of CS_2 towards DCF is much superior to that of VFX. This different affinity can be explained by the different electrostatic interactions established. Essentially, three parameters are needed to evaluate the electrostatic interactions established between the surface of CS_2 and a given OMP, namely the solution pH, the p*K*a of the OMP, and the pH_{PZC} of the adsorbate. Table 4.6 summarizes these parameters. As observed, the pH_{PZC} of CS_2 is 7.9. Thus, the surface of CS_2 is positively charged at the pH of

both solutions of DCF and VFX (pH < pH_{PZC} in both cases, as shown in Table 4.6). It is also found that the pH of the solution containing DCF (6.4) is higher than the p*K*a of this OMP (4.15), revealing that the DCF in solution is (partially) negatively charged. Therefore, electrostatic attraction is expected to occur between the negatively charged DCF and the positively charged surface of CS_2, which explains the higher adsorption performance of this material towards DCF. Contrarily, the pH of the solution containing VFX (6.2) is lower than the p*K*a of this OMP (10.09), revealing that the VFX in solution is (partially) positively charged. Consequently, some electrostatic repulsion is expected to occur between the positively charged VFX and the positively charged surface of CS_2, which explains the lower adsorption performance of this material towards VFX.

Table 4.6. Solution pH, p*K*a of each OMP, and pH_{PZC} of CS_2.

	pH	p*K*a	pH_{PCZ}
DCF	6.4 ± 0.1	4.15	7.9 ± 0.1
VFX	6.2 ± 0.1	10.09	

Additional experiments were performed to study the potential effect of the hollow core of CS_2 on the adsorption performance. On this regard, it was fundamental to understand whether the higher adsorption capacity revealed by CS_2, when compared to $SiO_2@CS_2$, was due to the higher carbon content of CS_2, or to the presence of the hollow core. Therefore, the information obtained from the TGA experiments (Table 4.2) was fundamental to compare the carbon content of each of these materials, and thus design an additional experiment to ascertain the hypotheses raised. Accordingly, the adsorbent concentration was normalized by the carbon content, as described in Eq. 12, where $C_{ads,C}$ (g L^{-1}) is the concentration of carbon, C_{ads} is the total adsorbent concentration, and *CC* is the carbon content obtained from TGA (Table 4.2).

$$C_{ads,C} = C_{ads} \cdot \frac{CC}{100} \quad (12)$$

The $C_{ads,C}$ obtained for CS_2 was 0.2425 g L^{-1}, which is 5.1-fold higher than that of $SiO_2@CS_2$ (0.0475 g L^{-1}). Therefore, an additional experiment was performed with a higher concentration of $SiO_2@CS_2$ (1.28 g L^{-1}), corresponding to the same $C_{ads,C}$ as that in the experiment performed with CS_2. The corresponding experimental results are shown in Figure 4.10 (duplicate experiments), as well as the model that best fits the experimental data for each OMP (the corresponding parameters are given in Table 4.7). The detailed kinetic data is detailed in Appendix D (Table D.2). Comparing the results shown in Figure 4.9 with those in Figure 4.10, it is observed that CS_2 (Figure 4.9) still performs better than $SiO_2@CS_2$ (Figure 4.10). Specifically, the maximum q_t obtained for DCF and VFX onto CS_2 was 102 and 36 mg g^{-1}, respectively, whereas

onto SiO_2@CS_2 it was 85 and 23 mg g^{-1}, respectively. Bearing this in mind, it can be concluded that the hollow core of CS_2 was, in fact, beneficial for the adsorption of both DCF and VFX, suggesting that these hollow carbon structures can be used as nanocontainers for OMPs.

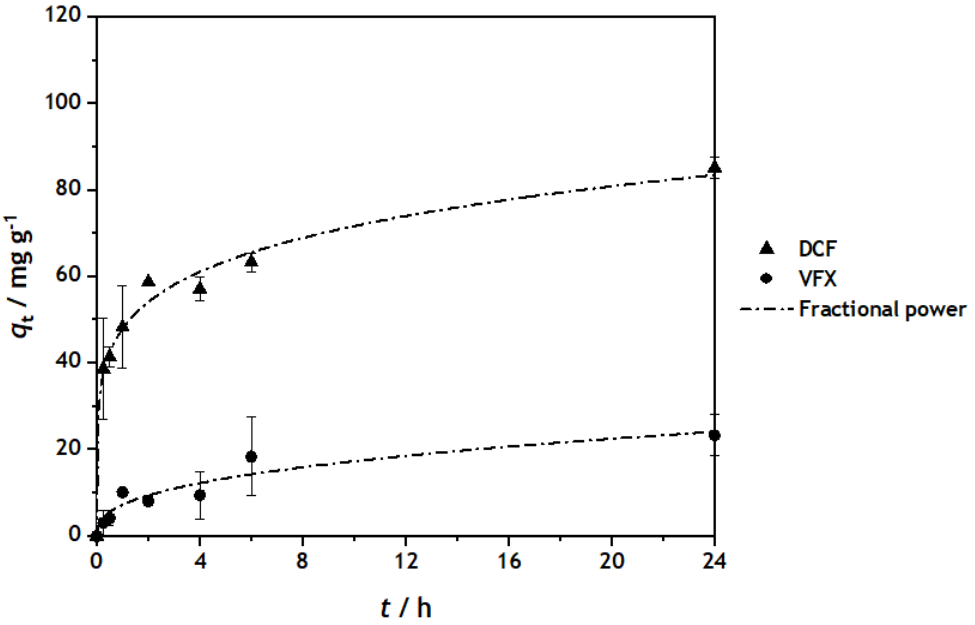


Figure 4.10. Kinetic experimental and theoretical data for the adsorption of DCF and VFX onto SiO_2@CS_2. Experiments performed with [SiO_2@CS_2] = 1.28 g L^{-1} (corresponding to $C_{ads,C}$ = 0.2425 g L^{-1}), $[DCF]_0$ or $[VFX]_0$ = 100 mg L^{-1}, pH = 6.4 or 6.2 (inherent pH of DCF and VFX solutions, respectively), T = 23 ± 1 °C (room temperature), and stirring speed of 200 rpm.

Table 4.7. Kinetic model parameters (non-linearized form equations) for the adsorption of DCF and VFX onto SiO_2@CS_2.

Fractional power model	a / mg g^{-1} h^{-1}	b	r^2
DCF	48.01	0.17	0.9890
VFX	7.27	0.38	0.9102
Lagergren pseudo-first order model	q_e / mg g^{-1}	k_1 / h^{-1}	r^2
DCF	64.91	2.25	0.8306
VFX	22.98	0.23	0.8708
Pseudo-second order model	q_e / mg g^{-1}	k_2 / g mg^{-1} h^{-1}	r^2
DCF	71.49	0.04	0.9028
VFX	25.96	0.01	0.8915
Elovich model	α / g mg^{-1} h^{-1}	β / mg g^{-1} h^{-1}	r^2
DCF	15.30	9.81	0.9799
VFX	1.34	4.41	0.8975

4.4. Equilibrium adsorption experiments

Equilibrium adsorption experiments were conducted with two main objectives, namely to (i) evaluate the adsorption capacity of the hollow CSs, and (ii) study the effect of particle size on the adsorption performance.

The equilibrium adsorption results obtained with the three hollow CSs are shown in Figure 4.11 and the detailed equilibrium data is detailed in Appendix E (Table E.1). Moreover, equilibrium modelling was performed as described in Section 3.4.1. Table 4.8 provides all the parameters related to the equilibrium models applied, as well as the corresponding r^2. Among the models studied, namely the non-linearized forms of the Langmuir, Freundlich, and Sips models (Eqs. 6-8), as somehow expected the Sips model was found to be the most suitable for fitting the experimental data. Therefore, the curves obtained with this model are shown in Figure 4.11.

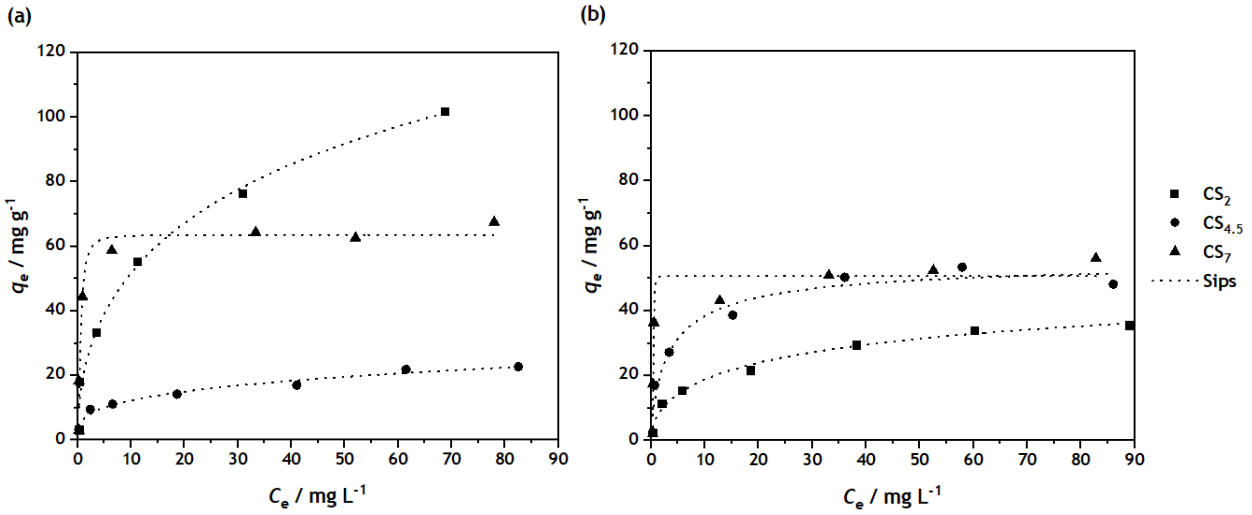


Figure 4.11. Experimental and theoretical data for the adsorption isotherms of (a) DCF and (b) VFX onto CS_2, $CS_{4.5}$ or CS_7. Experiments performed with $[CS_X]$ = 0.25 g L^{-1}, $[DCF]_0$ or $[VFX]_0$ = 1, 5, 10, 25, 50, 75, and 100 mg L^{-1}, T = 23 ± 1 ºC (room temperature), t = 24 h, and stirring speed of 200 rpm.

Overall, the adsorption capacity of the hollow CSs towards DCF is higher than the adsorption capacity towards VFX. As discussed in Section 4.3, this can be explained by the different electrostatic interactions established in each case (*i.e.*, some electrostatic attraction between the surface of the CSs and DCF, and some electrostatic repulsion between the surface of the CSs and VFX). Specifically, CS_2 and CS_7 reveal better adsorption capacity for DCF than $CS_{4.5}$ (Figure 4.11a). This may be explained by enhanced surface area and porosity of CS_2 and CS_7 when compared to $CS_{4.5}$ (Table 4.3). As for the adsorption of VFX (Figure 4.11b), $CS_{4.5}$ and CS_7 showed similar adsorption capacities, which were both higher than the adsorption capacity revealed by CS_2. These results cannot be explained by the different textural properties of the materials, nor by the electrostatic interactions previously discussed. Nevertheless, the higher

pH_{PZC} of $CS_{4.5}$ and CS_7 (≈ 10) compared to that of CS_2 (7.9), suggests that other adsorption mechanisms, such as chemisorption, may also be involved. The better adsorption performance over the concentration ranged under study was obtained with CS_7, regardless of the OMP considered. However, despite this better adsorption performance obtained with the hollow CSs with larger particle size (*i.e.*, CS_7, with $d_{average}$ of (284 ± 32) nm, as shown in Table 4.1), the effect of particle size was not very conclusive, since the effectiveness of the dissolution of the silica core was not the same for all the materials (as discussed throughout Section 4.2). Therefore, no evident correlations were obtained between the adsorption performance and the particle size of the hollow CSs.

Table 4.8. Equilibrium model parameters (non-linearized form equations) for the adsorption of DCF and VFX onto the hollow CSs.

	Langmuir			**Freundlich**			**Sips**			
	q_{sat} / mg g^{-1}	K_L / L mg^{-1}	r^2	K_F / L^{1/n_F} mg^{1-1/n_F} g^{-1}	n_F	r^2	q_m / mg g^{-1}	K_s / L^{n_S} mg^{-n_S}	n_S	r^2
DCF										
CS_2	109.66	0.10	0.9542	20.87	2.65	0.9840	259.80	0.01	2.04	0.9871
$CS_{4.5}$	21.81	0.19	0.8812	6.33	3.46	0.9769	56.84	3.77×10^{-3}	2.83	0.9769
CS_7	66.36	1.31	0.9312	31.03	5.15	0.7646	63.60	1.72	0.54	0.9608
VFX										
CS_2	37.05	0.12	0.9569	8.23	2.96	0.9792	61.45	0.02	1.87	0.9888
$CS_{4.5}$	51.69	0.37	0.9498	17.55	3.83	0.8914	56.02	0.27	1.30	0.9576
CS_7	52.32	1.39	0.8047	23.70	4.87	0.7726	50.64	2.21	0.19	0.9143

Regarding equilibrium modeling, the Sips model (3-parameter isotherm model) showed the highest values of r^2 (Table 4.8). This suggests that adsorption is taking place on both homogeneous and heterogeneous surface of the CSs. Among the 2-parameter isotherm models (*i.e.*, Freundlich and Langmuir), the Langmuir model was the best to predict the adsorption of both OMPs onto CS_7, and the Freundlich model was the most suitable to predict adsorption on CS_2. $CS_{4.5}$ revealed different behavior depending on the OMP considered; in this case, the adsorption of DCF and VFX was better described by the Freundlich and Langmuir models, respectively.

Tables 4.9 and 4.10 show the comparison of the performance of the CSs for removing DCF and VFX, respectively, with other carbon-based materials reported in the literature. Overall, the performances obtained with the CSs developed in this study are above the average of those previously reported, thus highlighting the potential of these hollow carbon nanocontainers as efficient adsorbents for DCF removal (Table 4.9). It is important to note that the higher capacities observed may be due, essentially, to the high surface area of the material or the change of pH of the solution or the change of the adsorbent concentration. The developed CSs, on the other hand, performed better compared to the materials tested in the only work found in the literature with VFX (Table 4.10).

Table 4.9. Comparison of the performance of several reported carbon-based materials developed as adsorbents of DCF [a].

Reference	Adsorbent	Adsorption conditions	S_{BET} / $m^2\ g^{-1}$	Maximum capacity / mg g^{-1}	Isotherm
This study	**CS_2**	Ultrapure water, $pH_{solution}$ = 6.4, C_{ads} =0.25 g L^{-1}, C_0 = 1 – 100 mg L^{-1}, T = 23 ºC, t = 24 h	545	259.80	Sips
	$CS_{4.5}$		271	56.84	Sips
	CS_7		602	63.60	Sips
Rigueto *et al.*, 2021 [52]	**Commercial gelatin powder with carbon nanotubes**	n/d, $pH_{solution}$ = 8.15, C_{ads} = 2.0 g L^{-1}, C_0 = 37.5 – 300 mg L^{-1}, T = 25 ºC, t = 2.5 h	133	26.97	Freundlich
Kimbi Yaah *et al.*, 2021 [53]	**Hydrochar-derived adsorbent**	Deionized water, $pH_{solution}$ = 2.0, C_{ads} = 15 g L^{-1}, C_0 = 0 – 50 mg L^{-1}, T = 25 ºC, t = 1.5 h	131	13.16	Langmuir
Salvestrini *et al.*, 2020 [54]	**Commercial activated carbon, Filtrasorb 400**	Pure water, $pH_{solution}$ = 6.8, C_{ads} = 0.5 g L^{-1}, C_0 = 24 - 218 mg L^{-1}, T = n/d, t = 120 h	1000	180	Langmuir
Khalil *et al.*, 2020 [55]	**Graphene**	n/d, $pH_{solution}$ = 7.5, C_{ads} = 0.25 g L^{-1}, C_0 = 0.1 - 100 mg L^{-1}, T = 22, t = 24 h	670	76	Sips
Álvarez-Torrellas *et al.*, 2018 [56]	**Carbide-derived carbons produced at 1000ºC**	Deionized water, $pH_{solution}$ = n/d, C_{ads} = 0.3 g L^{-1}, C_0 = 10 – 100 mg L^{-1}, T = 30 ºC, t = 1 h	1676	523	n/d
Jauris, *et al.*, 2016 [57]	**Reduced graphene oxide**	Deionized water, $pH_{solution}$ = 10.0, C_{ads} =1.5 g L^{-1}, C_0 = 20 - 200 mg L^{-1}, T = 25 ºC, t = 3.3 h	98	59.67	Liu *
Bhadra *et al.*, 2016 [58]	**Activated carbons oxidized with ammonium persulfate**	Water, $pH_{solution}$ = 5.5, C_{ads} = 0.2 g L^{-1}, C_0 = 25 – 100 mg L^{-1}, T = 25 ºC, t = 24 h	704	487	Langmuir
Bernardo *et al.*, 2016 [59]	**Potato peel waste-based activated carbon**	Deionized water, $pH_{solution}$ = 5, C_{ads} = 0.4 g L^{-1}, C_0 = 10 - 100 mg L^{-1}, T = 25 ºC, t = 17 h	866	68.5	Langmuir

[a] Data collected from Scopus on June 24, 2021, using the following query: "carbon AND adsorption AND diclofenac AND Chemical Engineering AND Environmental Science".

n/d no data.

* the authors used *Liu* as an isotherm model.

Table 4.10. Comparison of the performance of several reported carbon-based materials developed as adsorbents of VFX [a].

Reference	Adsorbent	Adsorption conditions	S_{BET} / $m^2\ g^{-1}$	Maximum capacity / mg g^{-1}	Isotherm
This study	**CS_2**	Ultrapure water, $pH_{solution}$ = 6.2, C_{ads} =0.25 g L^{-1}, C_0 = 1 – 100 mg L^{-1}, T = 23 ºC, t = 24 h	545	61.45	Sips
	$CS_{4.5}$		271	56.02	Sips
	CS_7		602	50.64	Sips
Calisto *et al.*, 2015 [60]	**Commercial activated carbon**	Ultrapure water, $pH_{solution}$ = 7.0, C_{ads} = 0.02 – 0.12 g L^{-1}, C_0 = 5 mg L^{-1}, T = 25 ºC, t = 0.5 h	848	42.5	Langmuir
	Non-activated carbon produced by pyrolysis of paper mill sludge	Ultrapure water, $pH_{solution}$ = 10.5, C_{ads} = 0.15 – 4.0 g L^{-1}, C_0 = 5 mg L^{-1}, T = 25 ºC, t = 0.5 h	209	8.5	Langmuir

[a] Data collected from Scopus on June 24, 2021, using the following query: "carbon AND adsorption AND venlafaxine AND Chemical Engineering AND Environmental Science".

n/d no data.

5. Conclusions

In this work, carbon-based materials with three different sizes were developed for the removal of DCF and VFX from aqueous solution. These materials showed a spherical morphology and the particle size increased by increasing of the E/W volumetric ratio. The average diameter of the SiO_2@CSs varied from 168 to 270 nm and the dominant element was silicon, while the CSs had an average diameter between 109 and 284 nm and carbon as the dominant element.

The etching process was more effective in the case of CS_2, followed by CS_7, and not as effective in the case of $CS_{4.5}$ (TGA residue ranging from 3 to 46 wt.%).

The S_{BET} of the CSs ranged from 271 to 602 $m^2\ g^{-1}$, making them more porous in comparison to SiO_2@CSs (S_{BET} in the range 115 to 144 $m^2\ g^{-1}$). The microporous and mesoporous structure of CSs were more pronounced than that of SiO_2@CSs. The pH_{PZC} of the CSs ranged from 8 to 10, revealing their basic character.

From the kinetic studies, it was possible to demonstrate the positive impact of the hollow core and that the adsorption process could reach the equilibrium within 24 h. Specifically, the adsorption capacity onto CS_2 was 102 and 36 mg g^{-1} for DCF and VFX, respectively, in contrast to SiO_2@CS_2, which had almost zero adsorption capacity. Moreover, it was found that the higher adsorption capacity of CS_2 was mainly due to the hollow core and not to the carbon fraction that this material possessed.

From the equilibrium studies, DCF adsorption capacities of 102, 23 and 68 mg g^{-1} were obtained for CS_2, $CS_{4.5}$ and CS_7, respectively, whereas the adsorption capacities of VFX were 36, 48 and 56 mg g^{-1}, for the same materials.

Moreover, adsorption kinetic data was well described by the pseudo-first order and power fractional kinetic model for DCF and for VFX, respectively, whereas the Sips model fitted well to the equilibrium data.

Equilibrium studies demonstrated that CS_7 was the one that presented the best compromise for the adsorption of both OMPs. Moreover, this carbon material presented the best removals at lower concentrations of adsorbate.

To conclude, the synthesized materials could be a promising material for environmental remediation, not only for DCF and VFX, but also for the removal of other organic compounds from water. However, additional studies are needed to better understand the performance of these materials with real water matrices rather than ultrapure water.

6. Assessment of the work

6.1. Objectives achieved

In general, the previously defined objectives were achieved since it was possible to develop the nanostructured carbon spheres with different particle sizes. Apart from the silica removal efficiency of the core of the CSs, which was not fully effective in $CS_{4.5}$ and CS_7. Obtaining the CSs allowed the following objectives to be achieved and fulfilled, such as, the characterization of all the materials, including morphological, textural, and surface chemistry properties. These CSs also enabled studies of adsorption of OMPs, and it was possible to see the effect of the hollow core, within the CSs, as well as to determine the equilibrium time. Regarding the objective of studying the effect of particle size on the adsorption performance, the results were not very conclusive, because no evident correlations were obtained between adsorption performance and the particle size of the hollow CSs.

The deviations obtained in these experiments were quite acceptable given the complex procedure involved from synthesis to adsorption tests. Specifically, some experimental artifacts that may have happened throughout the kinetics and equilibrium studies such as, the error of weighing very low masses of a heterogeneous material, the dilution of the solutions with the highest concentrations (> 25 mg L^{-1}) prior to analysis, the use of materials synthetized in different batch runs, the difficult and complex process of obtaining spheres without silica which involves several steps, adequate stirring speed, temperature variations, among others.

6.2. Other work carried out

While conducting the work needed to conclude the present dissertation, I was able to deliver the following (peer-reviewed) poster presentation (including a 1 min video for its presentation):

Luísa Vieira, Ana R. Lado Ribeiro, Rui S. Ribeiro, Adrián M.T. Silva, *Synthesis and characterization of nanostructured carbon spheres*, in: "DCE21 – 4th Doctoral Congress in Engineering", 28 – 29 June 2021, Porto, Portugal (online conference). Published in the Book of Abstracts of the conference (ISBN: 978-972-752-280-4), p. 113.

Moreover, one manuscript is currently under preparation for submission to an international peer-reviewed scientific journal.

6.3. Final assessment

The potential of using hollow CSs as adsorbents of OMPs was shown in the present dissertation, opening the possibility of continuing, developing better materials and delving into other environmental applications, such as:

- solid-liquid extraction for application in sample preparation of complex matrices (*e.g.*, sample concentration of OMPs and cleanup of environmental samples to be further analyzed by liquid or gas chromatography coupled to mass spectrometry);
- assessment of desorption from the carbon materials as an important step in sample preparation methodologies;
- solid-liquid extraction as an environmental remediation process to remove OMPs from water/wastewater;
- assessment of regeneration of the carbon materials as a crucial characteristic for adsorbents used in water/wastewater treatment.

It would also be interesting to employ these materials in electrochemical applications such as batteries or sensors, due to the fact that CSs offer excellent physical properties and high conductivities [61]. Additionally, it would be relevant to upscale the synthesis process, *i.e.*, to obtain more material in each synthesis batch run and thus have an adequate amount (of a more homogenous sample) for a complete round of experiments. Moreover, the NaOH etching step should be adjusted to the different diameters of the CSs, *i.e.*, the proportion of NaOH used should be higher for the larger spheres, in order to achieve a more efficient removal of the silica core. It would also be interesting to optimize the experimental conditions, such as solution pH and adsorbent concentration, and to study feasibility of using E/W volumetric ratio above 7.

References

1. Deblonde T, Cossu-Leguille C, Hartemann P. Emerging pollutants in wastewater: A review of the literature. *Int J Hyg Environ Health*. 2011;214(6):442-448. doi:10.1016/j.ijheh.2011.08.002
2. Gorito AM, Ribeiro AR, Almeida CMR, Silva AMT. A review on the application of constructed wetlands for the removal of priority substances and contaminants of emerging concern listed in recently launched EU legislation. *Environ Pollut*. 2017;227:428-443. doi:10.1016/j.envpol.2017.04.060
3. Sen TK. Physical Chemical and Biological Treatment Processes for Water and Wastewater. Published 2014. Accessed April 17, 2021. http://search.ebscohost.com/login.aspx?direct=true&AuthType=ip,uid&db=e230xww&AN=1084472&lang=pt-pt&site=ehost-live&scope=site
4. Von Sperling M. *Wastewater Characteristics, Treatment and Disposal*. Vol 6. IWA Publishing; 2015. doi:10.2166/9781780402086
5. Commission E. River basin management - Water - Environment. Accessed February 23, 2021. https://ec.europa.eu/environment/water/water-framework/index_en.html
6. Commission E. *The EU Water Framework Directive*.; 2010. Accessed February 23, 2021. http://ec.europa.eu/environment/pubs/pdf/factsheets/water-framework-directive.pdf
7. Giakoumis T, Voulvoulis N. The Transition of EU Water Policy Towards the Water Framework Directive's Integrated River Basin Management Paradigm. *Environ Manage*. 2018;62(5):819-831. doi:10.1007/s00267-018-1080-z
8. Sousa JCG, Ribeiro AR, Barbosa MO, Pereira MFR, Silva AMT. A review on environmental monitoring of water organic pollutants identified by EU guidelines. *J Hazard Mater*. 2018;344:146-162. doi:10.1016/j.jhazmat.2017.09.058
9. Rubirola A, Quintana J, Boleda MR, Galceran MT. Analysis of 32 priority substances from EU water framework directive in wastewaters, surface and drinking waters with a fast sample treatment methodology. *Int J Environ Anal Chem*. 2019;99(1):16-32. doi:10.1080/03067319.2019.1571195
10. Commission E. *Commission Implementing Decision (EU) 2020/1161*.; 2020. Accessed March 12, 2021. https://eur-lex.europa.eu/legal-content/EN/TXT/PDF/?uri=CELEX:32020D1161&from=EN
11. Ribeiro AR, Nunes OC, Pereira MFR, Silva AMT. An overview on the advanced oxidation processes applied for the treatment of water pollutants defined in the recently launched Directive 2013/39/EU. *Environ Int*. 2015;75:33-51. doi:10.1016/j.envint.2014.10.027
12. Nilsen E, Smalling KL, Ahrens L, et al. Critical review: Grand challenges in assessing the adverse effects of contaminants of emerging concern on aquatic food webs. *Environ Toxicol Chem*. 2019;38(1):46-60. doi:10.1002/etc.4290
13. Zhang Y, Geißen SU, Gal C. Carbamazepine and diclofenac: Removal in wastewater treatment plants and occurrence in water bodies. *Chemosphere*. 2008;73(8):1151-1161. doi:10.1016/j.chemosphere.2008.07.086
14. Pérez-Estrada LA, Malato S, Gernjak W, et al. Photo-fenton degradation of diclofenac: Identification of main intermediates and degradation pathway. *Environ Sci Technol*.

2005;39(21):8300-8306. doi:10.1021/es050794n

15. Lacorte S, Luis S, Gómez-Canela C, et al. Pharmaceuticals released from senior residences: occurrence and risk evaluation. *Environ Sci Pollut Res*. 2018;25(7):6095-6106. doi:10.1007/s11356-017-9755-1
16. Commission E. *European Union Strategic Approach to Pharmaceuticals in the Environment*.; 2019. Accessed March 7, 2021. https://eur-lex.europa.eu/legal-content/EN/TXT/PDF/?uri=CELEX:52019DC0128&from=EN
17. Parolini M. Toxicity of the Non-Steroidal Anti-Inflammatory Drugs (NSAIDs) acetylsalicylic acid, paracetamol, diclofenac, ibuprofen and naproxen towards freshwater invertebrates: A review. *Sci Total Environ*. 2020;740:140043. doi:10.1016/j.scitotenv.2020.140043
18. Minguez L, Di Poi C, Farcy E, et al. Comparison of the sensitivity of seven marine and freshwater bioassays as regards antidepressant toxicity assessment. *Ecotoxicology*. 2014;23(9):1744-1754. doi:10.1007/s10646-014-1339-y
19. Minagh E, Hernan R, O'Rourke K, Lyng FM, Davoren M. Aquatic ecotoxicity of the selective serotonin reuptake inhibitor sertraline hydrochloride in a battery of freshwater test species. *Ecotoxicol Environ Saf*. 2009;72(2):434-440. doi:10.1016/j.ecoenv.2008.05.002
20. Lima DLD, Silva CP, Otero M. Dispersive liquid-liquid microextraction for the quantification of venlafaxine in environmental waters. *J Environ Manage*. 2018;217:71-77. doi:10.1016/j.jenvman.2018.03.060
21. Llorca M, Castellet-Rovira F, Farré MJ, et al. Fungal biodegradation of the N-nitrosodimethylamine precursors venlafaxine and O-desmethylvenlafaxine in water. *Environ Pollut*. 2019;246:346-356. doi:10.1016/j.envpol.2018.12.008
22. Hartmann J, Bartels P, Mau U, et al. Degradation of the drug diclofenac in water by sonolysis in presence of catalysts. *Chemosphere*. 2008;70(3):453-461. doi:10.1016/j.chemosphere.2007.06.063
23. Arlos MJ, Bragg LM, Servos MR, Parker WJ. Simulation of the fate of selected pharmaceuticals and personal care products in a highly impacted reach of a Canadian watershed. *Sci Total Environ*. 2014;485-486(1):193-204. doi:10.1016/j.scitotenv.2014.03.092
24. Koutsouba V, Heberer T, Fuhrmann B, Schmidt-Baumler K, Tsipi D, Hiskia A. Determination of polar pharmaceuticals in sewage water of Greece by gas chromatography-mass spectrometry. *Chemosphere*. 2003;51(2):69-75. doi:10.1016/S0045-6535(02)00819-6
25. SpectraBase. Accessed March 13, 2021. https://spectrabase.com/
26. DrugBank. Accessed March 13, 2021. https://go.drugbank.com/
27. PubChem. Accessed March 13, 2021. https://pubchem.ncbi.nlm.nih.gov/
28. Holliday SM, Benfield P. Venlafaxine: A Review of its Pharmacology and Therapeutic Potential in Depression. *Drugs*. 1995;49(2):280-294. doi:10.2165/00003495-199549020-00010
29. Homlok R, Takács E, Wojnárovits L. Elimination of diclofenac from water using irradiation technology. *Chemosphere*. 2011;85(4):603-608. doi:10.1016/j.chemosphere.2011.06.101
30. Sathishkumar P, Meena RAA, Palanisami T, Ashokkumar V, Palvannan T, Gu FL. Occurrence, interactive effects and ecological risk of diclofenac in environmental compartments and biota - a review. *Sci Total Environ*. 2020;698:134057. doi:10.1016/j.scitotenv.2019.134057

31. Commission E. *Commission Implementing Decision (EU) 2015/ 495*.; 2015. Accessed March 10, 2021. https://eur-lex.europa.eu/legal-content/EN/TXT/PDF/?uri=CELEX:32015D0495&from=EN
32. Feito R, Valcárcel Y, Catalá M. Preliminary data suggest that venlafaxine environmental concentrations could be toxic to plants. *Chemosphere*. 2013;90(7):2065-2069. doi:10.1016/j.chemosphere.2012.09.028
33. Khajeh M, Laurent S, Dastafkan K. Nanoadsorbents: Classification, preparation, and applications (with emphasis on aqueous media). *Chem Rev*. 2013;113(10):7728-7768. doi:10.1021/cr400086v
34. Wang J, Guo X. Adsorption isotherm models: Classification, physical meaning, application and solving method. *Chemosphere*. 2020;258:127279. doi:10.1016/j.chemosphere.2020.127279
35. Tripathy M, Padhiari S, Hota G. L-Cysteine-Functionalized Mesoporous Magnetite Nanospheres: Synthesis and Adsorptive Application toward Arsenic Remediation. *J Chem Eng Data*. 2020;65(8):3906-3919. doi:10.1021/acs.jced.0c00250
36. Fuertes AB, Valle-Vigón P, Sevilla M. One-step synthesis of silica@resorcinol-formaldehyde spheres and their application for the fabrication of polymer and carbon capsules. *Chem Commun*. 2012;48(49):6124-6126. doi:10.1039/c2cc32552g
37. Thommes M, Kaneko K, Neimark A V., et al. Physisorption of gases, with special reference to the evaluation of surface area and pore size distribution (IUPAC Technical Report). *Pure Appl Chem*. 2015;87(9-10):1051-1069. doi:10.1515/pac-2014-1117
38. Ribeiro RS, Frontistis Z, Mantzavinos D, et al. Magnetic carbon xerogels for the catalytic wet peroxide oxidation of sulfamethoxazole in environmentally relevant water matrices. *Appl Catal B Environ*. 2016;199:170-186. doi:10.1016/j.apcatb.2016.06.021
39. Álvarez-Torrellas S, Ribeiro RS, Gomes HT, Ovejero G, García J. Removal of antibiotic compounds by adsorption using glycerol-based carbon materials. *Chem Eng J*. 2016;296:277-288. doi:10.1016/j.cej.2016.03.112
40. Seader JD, Henley EJ, Roper DK. *Separation Process Principles- Chemical and Biochemical Operations*. 3rd ed. John Wiley and Sons Ltd; 2011.
41. Gautam RK, Chattopadhyaya MC. Kinetics and Equilibrium Isotherm Modeling: Graphene-Based Nanomaterials for the Removal of Heavy Metals From Water. In: *Nanomaterials for Wastewater Remediation*. Elsevier; 2016:79-109. doi:10.1016/b978-0-12-804609-8.00005-4
42. Stöber W, Fink A, Bohn E. Controlled growth of monodisperse silica spheres in the micron size range. *J Colloid Interface Sci*. 1968;26(1):62-69. doi:10.1016/0021-9797(68)90272-5
43. Bogush GH, Zukoski IV CF. Studies of the kinetics of the precipitation of uniform silica particles through the hydrolysis and condensation of silicon alkoxides. *J Colloid Interface Sci*. 1991;142(1):1-18. doi:10.1016/0021-9797(91)90029-8
44. Chen SL, Dong P, Yang GH, Yang JJ. Kinetics of Formation of Monodisperse Colloidal Silica Particles through the Hydrolysis and Condensation of Tetraethylorthosilicate. *Ind Eng Chem Res*. 1996;35(12):4487-4493. doi:10.1021/ie9602217
45. Rao KS, El-Hami K, Kodaki T, Matsushige K, Makino K. A novel method for synthesis of silica nanoparticles. *J Colloid Interface Sci*. 2005;289(1):125-131. doi:10.1016/j.jcis.2005.02.019
46. Harris MT, Brunson RR, Byers CH. The base-catalyzed hydrolysis and condensation reactions of dilute and concentrated TEOS solutions. *J Non Cryst Solids*. 1990;121(1-3):397-403.

doi:10.1016/0022-3093(90)90165-I

47. Kim KS, Kim JK, Kim WS. Influence of reaction conditions on sol-precipitation process producing silicon oxide particles. *Ceram Int*. 2002;28(2):187-194. doi:10.1016/S0272-8842(01)00076-1
48. Van Blaaderen A, Van Geest J, Vrij A. Monodisperse colloidal silica spheres from tetraalkoxysilanes: Particle formation and growth mechanism. *J Colloid Interface Sci*. 1992;154(2):481-501. doi:10.1016/0021-9797(92)90163-G
49. Lu AH, Hao GP, Sun Q. Can carbon spheres be created through the stöber method? *Angew Chemie - Int Ed*. 2011;50(39):9023-9025. doi:10.1002/anie.201103514
50. Szekeres M, Tóth J, Dékány I. Specific surface area of stoeber silica determined by various experimental methods. *Langmuir*. 2002;18(7):2678-2685. doi:10.1021/la011370j
51. Rodríguez-Reinoso F. The role of carbon materials in heterogeneous catalysis. *Carbon N Y*. 1998;36(3):159-175. doi:10.1016/S0008-6223(97)00173-5
52. Rigueto CVT, Rosseto M, Nazari MT, et al. Adsorption of diclofenac sodium by composite beads prepared from tannery wastes-derived gelatin and carbon nanotubes. *J Environ Chem Eng*. 2021;9(1):105030. doi:10.1016/j.jece.2021.105030
53. Kimbi Yaah VB, Zbair M, Botelho de Oliveira S, Ojala S. Hydrochar-derived adsorbent for the removal of diclofenac from aqueous solution. *Nanotechnol Environ Eng*. 2021;6(1):3. doi:10.1007/s41204-020-00099-5
54. Salvestrini S, Fenti A, Chianese S, Iovino P, Musmarra D. Diclofenac sorption from synthetic water: Kinetic and thermodynamic analysis. *J Environ Chem Eng*. 2020;8(5):104105. doi:10.1016/j.jece.2020.104105
55. Khalil AME, Memon FA, Tabish TA, Salmon D, Zhang S, Butler D. Nanostructured porous graphene for efficient removal of emerging contaminants (pharmaceuticals) from water. *Chem Eng J*. 2020;398:125440. doi:10.1016/j.cej.2020.125440
56. Álvarez-Torrellas S, Munoz M, Gläsel J, et al. Highly efficient removal of pharmaceuticals from water by well-defined carbide-derived carbons. *Chem Eng J*. 2018;347:595-606. doi:10.1016/j.cej.2018.04.127
57. Jauris IM, Matos CF, Saucier C, et al. Adsorption of sodium diclofenac on graphene: A combined experimental and theoretical study. *Phys Chem Chem Phys*. 2016;18(3):1526-1536. doi:10.1039/c5cp05940b
58. Bhadra BN, Seo PW, Jhung SH. Adsorption of diclofenac sodium from water using oxidized activated carbon. *Chem Eng J*. 2016;301:27-34. doi:10.1016/j.cej.2016.04.143
59. Bernardo M, Rodrigues S, Lapa N, et al. High efficacy on diclofenac removal by activated carbon produced from potato peel waste. *Int J Environ Sci Technol*. 2016;13(8):1989-2000. doi:10.1007/s13762-016-1030-3
60. Calisto V, Ferreira CIA, Oliveira JABP, Otero M, Esteves VI. Adsorptive removal of pharmaceuticals from water by commercial and waste-based carbons. *J Environ Manage*. 2015;152:83-90. doi:10.1016/j.jenvman.2015.01.019
61. Zhang J, Ma J, Zhang S, Wang W, Chen Z. A highly sensitive nonenzymatic glucose sensor based on CuO nanoparticles decorated carbon spheres. *Sensors Actuators, B Chem*. 2015;211:385-391. doi:10.1016/j.snb.2015.01.100

Appendix A — Synthesis of CSs

The detailed synthesis parameters are given in Table A.1.

Table A.1. Amounts of reactants used in the synthesis of the SiO_2@RF spheres.

Sample	NH_4OH / mL	EtOH / mL	H_2O / mL	TEOS / mL	Resorcinol / g	Formaldehyde solution / mL
$SiO_2@RF_2$	5.00	107	53	5.60	0.805	1.12
$SiO_2@RF_{4.5}$	5.00	131	29	5.60	0.804	1.12
$SiO_2@RF_7$	5.00	140	20	5.60	0.801	1.12

Carbonization of SiO_2@RF spheres

From Eq. 1 (Section 3.2), it was possible to calculate the burn-off (*BO*) due to the thermal treatment performed to carbonize the polymeric spheres. Thus, *BO* of CS_2, $CS_{4.5}$ and CS_7 was 18, 25, and 22%, respectively.

Preparation of sodium hydroxide solution for the etching process

Sodium hydroxide (NaOH; *MW* = 39.997 g mol^{-1}) is a strong base and its preparation in water with a concentration of 10 mol L^{-1} involves a highly exothermic reaction. Therefore, the basic solution was prepared in a glass flask immersed in an ice bath. After dissolution of NaOH pellets, the solution was transferred to a volumetric flask. The weighing of NaOH was performed in a precision balance.

Etching process

The volume of NaOH solution needed for the etching of the silica from the core of the CSs was determined as described in Eq. 13, where V_{NaOH} (mL) is the volume of NaOH solution for each tested material.

$$V_{NaOH} = \frac{50 \text{ mL of NaOH}}{1 \text{ g of } SiO_2@CS} \times m_{SiO_2@CS} \quad (13)$$

Appendix B — Characterization techniques

Preparation of the sodium chloride solution for the pH drift tests (determination of pH_{PZC})

Sodium chloride (NaCl; *MW* = 58.44 g mol^{-1}) solution with a concentration of 0.01 mol L^{-1} was prepared with distilled water in a 2 L volumetric flask. The weighing of NaCl was performed in an analytical balance.

The NaCl solution was then divided into 5 flasks of 500 mL and the pH adjustment made with HCl or NaOH solutions (1.0 mol L^{-1}).

SEM images

The histograms of particle size distribution given in Figure B.1 were obtained by conducting at least 75 measurements in the respective SEM micrographs.

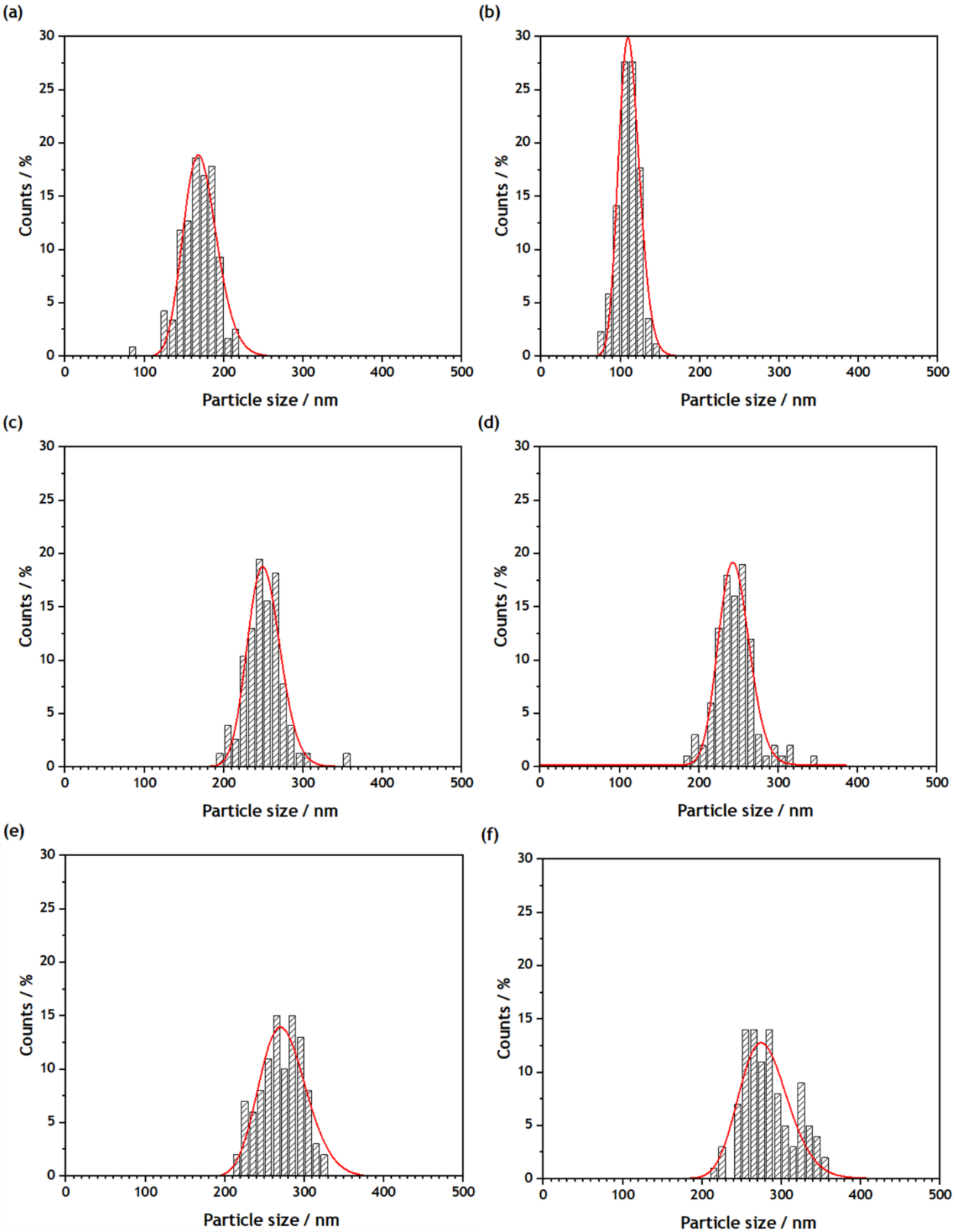


Figure B.1. Histogram of particle size distribution of: (a) $SiO_2@CS_2$, (b) CS_2, (c) $SiO_2@CS_{4.5}$, (d) $CS_{4.5}$, (e) $SiO_2@CS_7$, and (f) CS_7 as determined by SEM measurements. Red curves represent a log-normal distribution.

Textural characterization

The N_2 adsorption–desorption isotherms of the tested materials are shown in Figure B.2.

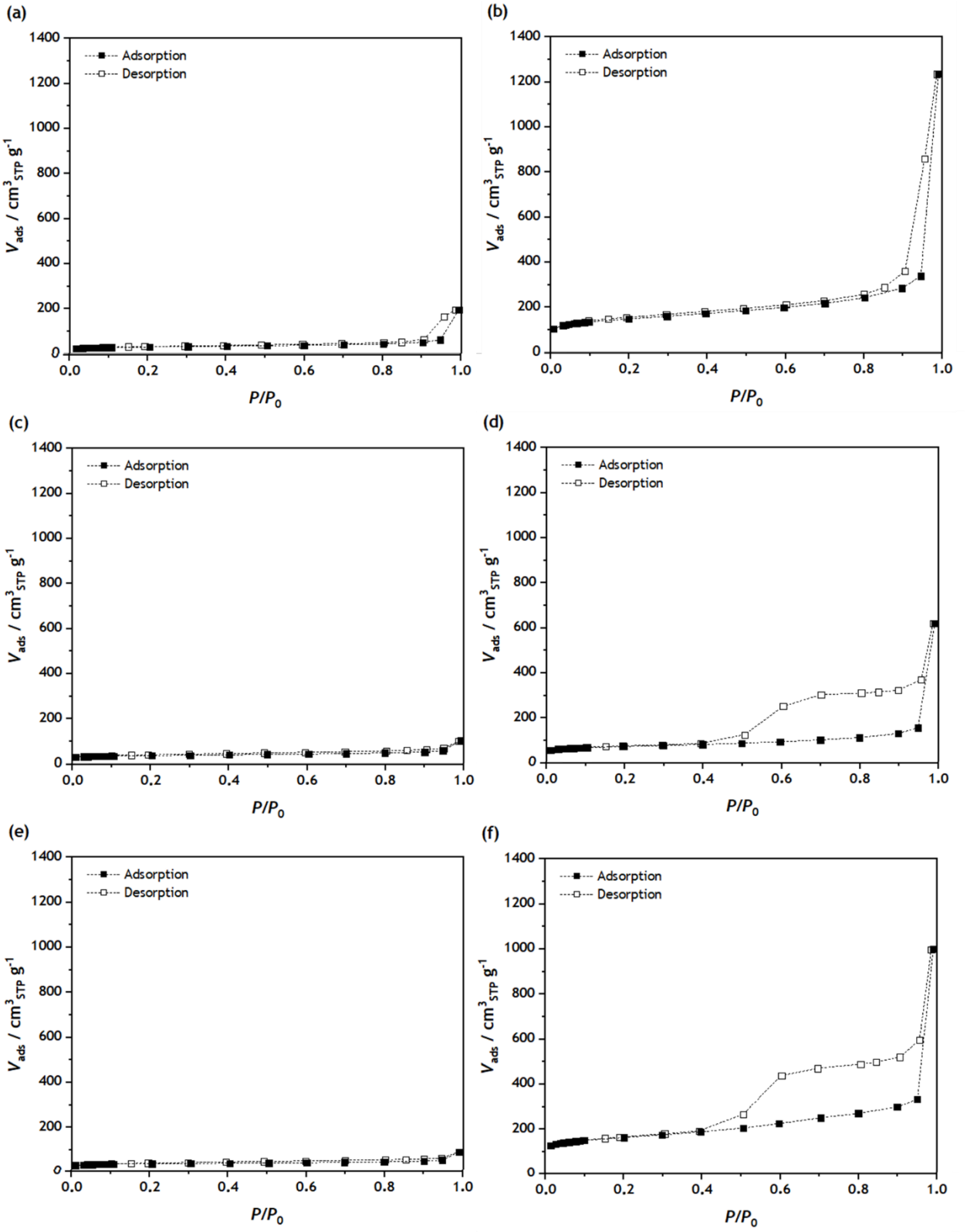


Figure B.2. Nitrogen adsorption-desorption isotherms at – 196 °C of: (a) $SiO_2@CS_2$, (b) CS_2, (c) $SiO_2@CS_{4.5}$, (d) $CS_{4.5}$, (e) $SiO_2@CS_7$, and (f) CS_7.

Surface chemistry characterization

pH_{PZC} is expressed by the point at which the experimental curve ($pH_{initial}$ versus pH_{final}) intersects the straight line given by $pH_{initial} = pH_{final}$, as shown in Figure B.3.

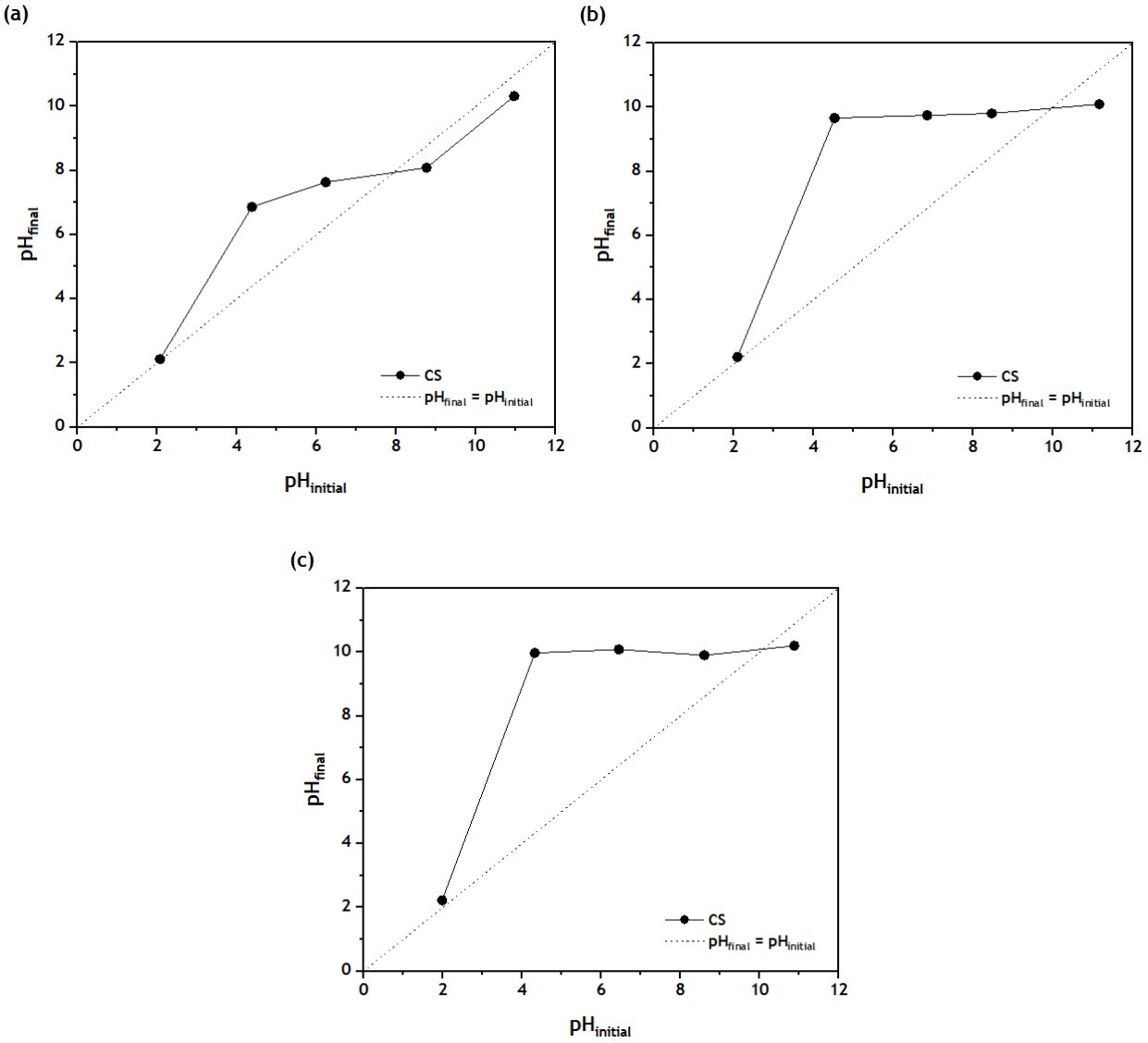


Figure B.3. Plot of final pH versus initial pH for determination of the pH_{PZC} of: (a) CS_2, (b) $CS_{4.5}$, and (c) CS_7.

Appendix C — Calibration curves

Preparation of DCF and VFX stock solutions

The diclofenac and venlafaxine stock solutions were prepared by weighing respectively ~32 mg of diclofenac sodium and ~34 mg of venlafaxine hydrochloride, which were individually diluted with ultrapure water, and then transferred to 2 different 100.00 mL volumetric flasks. The exact concentrations of the stock solutions of DCF and VFX obtained were 309.99 and 300.59 mg L^{-1}, respectively.

Preparation of standard solutions

Duplicates of ten standard solutions with concentrations of 100, 250, 500, 1000, 2500, 5000, 7500, 10000, 15000 and 25000 µg L^{-1}, were prepared. These standard solutions were obtained from a dilute solution with a concentration of 25000 µg L^{-1} that was prepared in a 10.00 mL volumetric flask, by adding the desired volumes of the DCF or VFX stock solutions and filling the remaining volume with ultrapure water. To plot the calibration curves applied for determination of both DCF and VFX, a Shimadzu HPLC apparatus with a fluorescence detector was used to analyze the analytes present in the prepared standard solutions. Each peak corresponds to a given component that absorbs and emits at selected wavelengths and whose area (*A*) is directly related to the concentration of that component.

Figure C.1 shows a chromatogram of the two analytes studied in this work, namely VFX and DCF. The first eluting peak corresponds to VFX, the second eluting peak corresponds to DCF. The retention time that each analyte takes to reach the detector after sample injection, is approximately 4.3 min for VFX and 9.2 min for DCF.

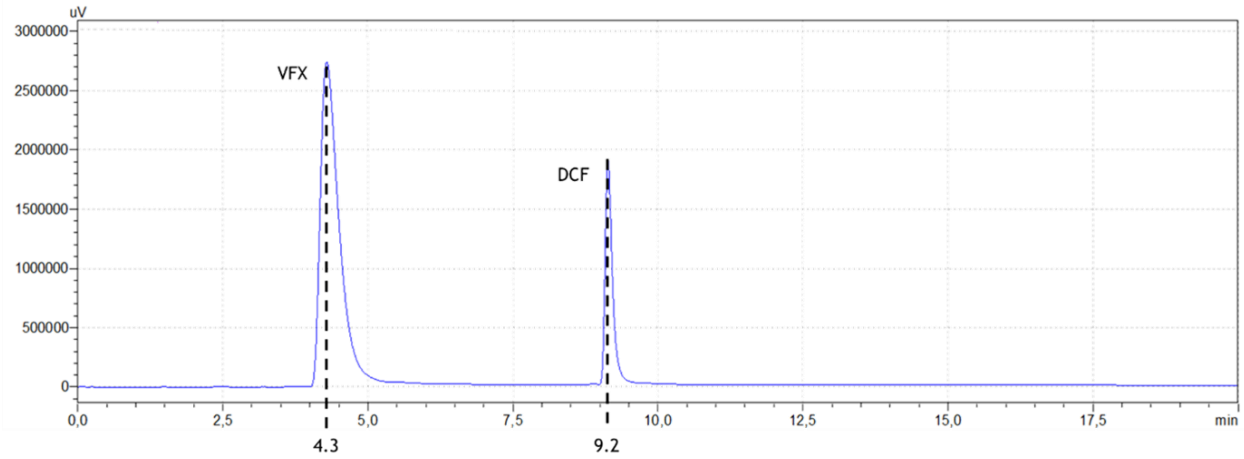


Figure C.1. Chromatogram for a two-component mixture of the detector signal (µV) as a function of time (min).

The equation of the calibration curve for the standard solutions of VFX from 100 to 25000 μg L^{-1} is given by Eq. 14, and that for the standard solutions of DCF from 250 to 25000 μg L^{-1} is given by Eq. 15, where $A_{average}$ (a.u.) is the average area and C (μg L^{-1}) is the concentration of VFX or DCF, respectively.

$$A_{average} = 8346 \cdot C_{VFX} + 840921 \quad (14)$$

$$A_{average} = 2547 \cdot C_{DCF} - 86113 \quad (15)$$

Method characterization

Linearity was controlled in the range of 100 to 25000 μg L^{-1}, and 250 to 10000 μg L^{-1} for VFX and DCF, respectively (injected standard solutions). Table C.1 details the figures of merit that were obtained for each calibration curve.

Table C.1. Correlation coefficient (r^2), limit of detection (LOD) and limit of quantitation (LOQ).

Parameter	VFX	DCF
r^2	0.9998	0.9996
LOD / μg L^{-1}	345	248
LOQ / μg L^{-1}	1150	828

Precision

The precision of an analytical procedure expresses the closeness between a series of measurements obtained from multiple analyses of the same sample. Precision has been considered at two levels: repeatability and reproducibility.

Method precision (Repeatability)

Five solutions containing 10000 μg L^{-1} of DCF or VFX were analyzed to check the repeatability response of the method. The relative standard deviation (RSD) of the method was calculated from the area obtained in each chromatogram (Table C.2). The RSD was 2.57 and 1.87% for VFX and DCF, respectively, which showed that the values are within the acceptable range (less than 5%) and that the method was precise.

Table C.2. Repeatability of the method.

C / µg L^{-1}	A_{VFX} / a.u.	A_{DCF} / a.u.
10000	78 871 582	24 208 539
10000	83 569 816	24 492 632
10000	85 274 289	24 438 047
10000	83 144 064	24 601 360
10000	83 500 740	23 350 903
Average / a.u.	82 872 098	24 218 296
RSD / %	2.57	1.87

Intermediate precision (Reproducibility)

Intermediate precision expressed within laboratory variations was studied in 3 different days, with 3 injections performed in each day for each standard solution. This study was carried out to determine the ruggedness of the proposed method.

The standard solutions were chosen based on the LOQ shown in Table C.1, *i.e.*, for VFX and DCF the standard solutions concentrations were 5000, 7500 and 15000 µg L^{-1}. No significant changes were observed in the chromatograms obtained in the inter-day study, thus proving that the method was rugged (Table C.3 and Table C.4).

Table C.3. Intermediate precision for the analysis of VFX in standard solutions (3 days, 3 replicates per day).

C / µg L^{-1}	$A_{average}^{n=1}$ / a.u.	$A_{average}^{n=2}$ / a.u.	$A_{average}^{n=3}$ / a.u.	Average / a.u.	RSD / %
5000	42 286 871	42 113 065	43 006 751	42 468 896	0.23
7500	63 399 648	61 886 950	63 842 166	63 042 922	0.59
15000	124 016 626	127 181 002	124 907 629	125 368 419	0.12

Table C.4. Intermediate precision for the analysis of DCF in standard solutions (3 days, 3 replicates per day).

C / µg L^{-1}	$A_{average}^{n=1}$ / a.u.	$A_{average}^{n=2}$ / a.u.	$A_{average}^{n=3}$ / a.u.	Average / a.u.	RSD / %
5000	12 048 378	12 915 679	11 720 837	12 228 298	0.59
7500	17 945 161	18 612 085	17 287 952	17 948 399	0.96
15000	35 066 832	35 702 695	32 859 808	34 543 111	0.31

Appendix D — Kinetics adsorption data

The adsorption capacity was determined using Eq. 16, considering the difference in solution concentration at the beginning (C_0) and over time (C_t), whereas V (mL) represents the solution volume and m_{ads} (g) is the mass of adsorbent.

$$q_t = \frac{(C_0 - C_t) \cdot V}{m_{ads}} \quad (16)$$

The experimental data given in Tables D.1 and D.2 are those presented graphically in Figures 4.9 and 4.10, respectively, and the removal efficiency of each pollutant by a given treatment was determined by using Eq. 17, where E (%) is the removal efficiency.

$$E = \frac{C_0 - C_t}{C_0} \times 100 \quad (17)$$

Therefore, the removal efficiency data is also given in Tables D.1 and D.2.

Table D.1. Average concentration (C), average adsorption capacity (q_t) and its standard deviation (σ), and removal efficiency (E) for CS_2 in DCF and VFX solutions. Experiments performed with C_{ads} = 0.25 g L^{-1}, pH = 6.4 or 6.2 (inherent pH of DCF and VFX solutions, respectively), T = 23 ± 1 ºC (room temperature), and stirring speed of 200 rpm.

Essay	t / h	C / mg L^{-1}	q_t / mg g^{-1}	σ / mg g^{-1}	E / %
DCF	0	94.2	n.a.	n.a.	n.a.
	0.25	83.2	80.1	2.6	12
	0.5	70.1	96.4	1.8	26
	1	68.0	104.7	2.9	28
	2	69.4	99.2	2.8	26
	4	66.9	109.1	6.9	29
	6	67.6	106.4	5.4	28
	24	68.7	102.0	2.1	27
VFX	0	98.0	n.a.	n.a.	n.a.
	0.25	91.8	24.7	3.0	6
	0.5	91.8	24.6	2.3	6
	1	89.0	28.3	0.0	9
	2	90.5	29.8	2.6	8
	4	91.8	24.7	2.4	6
	6	92.2	23.2	2.2	6
	24	89.1	35.6	2.2	9

n.a. Not applicable

Table D.2. Average concentration (C), average adsorption capacity (q_t) and its standard deviation (σ), and removal efficiency (E) for SiO_2@CS_2 in DCF and VFX solutions. Experiments performed with C_{ads} = 1.28 g L^{-1} (corresponding to $C_{ads,C}$ = 0.2425 g L^{-1}), pH = 6.4 or 6.2 (inherent pH of DCF and VFX solutions, respectively), T = 23 ± 1 ºC (room temperature), and stirring speed of 200 rpm.

Essay	t / h	C / mg L^{-1}	q_t / mg g^{-1}	σ / mg g^{-1}	E / %
DCF	0	87.0	n.a.	n.a.	n.a.
	0.25	77.3	38.6	11.7	11
	0.5	76.6	41.4	2.3	12
	1	74.9	48.3	9.5	14
	2	72.3	58.8	0.1	17
	4	72.7	57.2	2.7	16
	6	71.1	63.4	2.2	18
	24	65.7	85.2	2.5	24
VFX	0	98.5	n.a.	n.a.	n.a.
	0.25	97.7	3.1	2.9	1
	0.5	97.5	4.1	1.7	1
	1	96.0	10.2	0.8	3
	2	96.9	8.1	0.0	2
	4	96.1	9.5	5.5	2
	6	94.4	18.4	9.0	4
	24	92.7	23.3	4.7	6

n.a. Not applicable

Appendix E — Equilibrium adsorption data

The experimental data given in Table E.1 is that presented graphically in Figure 4.11. The removal efficiency of a pollutant was determined by using Eq. 17 and the values of *E* are presented in Table E.2, which were obtained from the data in Table E.1.

In the equilibrium experiments of CS_2, the assay with a C_0 of 75 mg L^{-1} was excluded from the graphical representation (Figure 4.11a) and from the theoretical model calculations since it seemed to be affected by any experimental artifact mentioned in Section 6.1.

Table E.1. Initial concentration (C_0), equilibrium concentration (C_e), equilibrium adsorption (q_e), and removal efficiency (E) for CS_2, $CS_{4.5}$ and CS_7 in DCF and VFX solutions. Experiments performed with C_{ads} = 0.25 g L^{-1}, T = 23 ± 1 ºC (room temperature), t = 24 h, and stirring speed of 200 rpm.

	CS_2				$CS_{4.5}$				CS_7			
	C_0 / mg L^{-1}	C_e / mg L^{-1}	q_e / mg g^{-1}	E / %	C_0 / mg L^{-1}	C_e / mg L^{-1}	q_e / mg g^{-1}	E / %	C_0 / mg L^{-1}	C_e / mg L^{-1}	q_e / mg g^{-1}	E / %
DCF	1.1	0.2	3.3	77	1.1	0.2	3.2	76	1.0	0.2	3.0	75
	4.9	0.4	18.1	93	4.8	2.4	9.5	50	4.8	0.2	18.3	95
	11.8	3.5	33.4	71	9.4	6.6	11.2	30	12.0	0.9	44.5	93
	25.0	11.2	55.3	55	22.2	18.6	14.3	16	21.1	6.4	58.7	70
	50.0	30.9	76.5	38	45.3	41.0	17.0	9	49.4	33.3	64.4	33
	-	-	-	-	67.0	61.5	21.9	8	67.7	52.0	62.6	23
	94.2	68.7	102.0	27	88.2	82.5	22.8	6	94.9	78.0	67.5	18
VFX	1.0	0.3	2.5	65	1.0	0.3	2.5	65	0.9	0.3	2.1	60
	4.9	2.0	11.4	59	5.0	0.7	17.1	86	4.7	0.3	17.5	93
	9.6	5.7	15.5	40	10.2	3.4	27.2	67	9.6	0.5	36.4	94
	24.0	18.5	21.8	23	24.9	15.2	38.7	39	23.6	12.8	43.1	46
	45.6	38.2	29.6	16	48.6	36.1	50.4	26	45.8	33.1	50.9	28
	69.1	60.2	34.0	13	71.3	57.9	53.5	19	65.6	52.5	52.4	20
	98.0	89.1	35.6	9	98.1	86.0	48.2	12	96.8	82.8	56.1	14